ELSEVIER

Contents lists available at ScienceDirect

Chemical Geology

journal homepage: www.elsevier.com/locate/chemgeo





U-series and Sr isotopes as tracers of mineral weathering and water routing from the deep Critical Zone to streamflow in a high-elevation volcanic catchment

Alissa White a,*, Lin Ma b, Bryan Moravec c, Jon Chorover c, Jennifer McIntosh a

- ^a Department of Hydrology and Atmospheric Sciences, University of Arizona, Tucson 85721, USA
- b Department of Geological Sciences, University of Texas at El Paso, El Paso 79968, USA
- ^c Department of Environmental Science, University of Arizona, Tucson 85721, USA

ARTICLE INFO

Keywords: Uranium-series activity ratios Radiogenic strontium isotopes Chemical weathering Isotope mixing analysis Groundwater contribution to streamflow Water routing

ABSTRACT

Tracing water routing and groundwater contribution to streamflow is a key tool for better understanding limited water resources. Measurements of U-series activity ratios and radiogenic Sr isotope ratios in drill cores, streams, and groundwater samples were employed to investigate weathering controls and better understand hydrologic flow paths and evolution through the heterogenous subsurface of a montane catchment. Situated within the semi-arid geologically complex volcanic setting of the Valles Caldera National Preserve in northern NM, this study focuses on streams draining the tallest (3432 masl) resurgent dome (Redondo Peak). Recent drilling of groundwater monitoring wells allowed for the collection and isotopic analysis of intact continuous cores and groundwater collected from similar depths, a unique and valuable contribution to U-series studies, within a high elevation headwater catchment focusing on two hillslopes with contrasting Critical Zone (CZ) structure and several distinct groundwater stores.

U-series composition of core samples identified U—Th fractionation from recent (< 1.25 Ma) disturbance in both hillslopes; however, (234 U/ 238 U) and (230 Th/ 238 U) disequilibria and 87 Sr/ 86 Sr values indicated more intense weathering and lithologic complexity in the hillslope underlain by volcanic breccia over vesicular tuff compared to the hillslope underlain by fractured tuff. The weathering profile of the site composed of breccia overlying vesicular tuff was influenced by the presence of shallow groundwater situated above deeper groundwater stores, which have distinctively higher (234 U/ 238 U) activity ratios and 87 Sr/ 86 Sr signatures than those of the deep groundwater stores in the fractured tuff site. The combination of U-series and Sr isotopes across time and in isotope mixing analysis highlights the utility of pairing these two isotope tracers that pinpoint distinct groundwater stores and help to isolate controls on U-series isotopes. Time series of U and Sr isotope signatures of groundwater and surface water suggest small seasonal changes in composition of streamflow while U—Sr isotope mixing analysis suggests that deep groundwater from the fractured tuff aquifer system generates more than 90% of streamflow to the greater catchment whereas shallow groundwater and soil water contribute less than 10% to streamflow, primarily following spring snowmelt. Importantly, constraining streamflow sources using isotope mixing analysis highlights that deep groundwater from fractured bedrock within the CZ sustains streamflow here and emphasizes the need to consider deep groundwater in future studies of fractured bedrock systems.

1. Introduction

Quantifying groundwater contribution to streamflow is an important challenge in hydrologic science, with particular relevance to projections of a warming climate and changes in precipitation frequency and timing, which threaten water resources (Barnett et al., 2005). While some

studies have suggested that deep groundwater contributes to streamflow (Paces et al., 2002; Liu et al., 2008; Welch and Allen, 2014; Frisbee et al., 2017), lack of access to deep groundwater and characterization of the deep subsurface in remote settings has made it difficult to study its contribution to streamflow. However, recent efforts focused on investigating the deep critical zone (CZ) have highlighted that understanding

^{*} Corresponding author at: 1133 E James E Rogers Way Harshbarger Bldg, Rm 122, Tucson, AZ 85721, USA. *E-mail address:* alissawhite@email.arizona.edu (A. White).

Chemical Geology 570 (2021) 120156

weathering processes at work in fractured bedrock that create storage, produce subsurface flow paths, and release solutes (Lebedeva and Brantley, 2013; Rempe and Dietrich, 2014; St. Clair et al., 2015; Brantley et al., 2017; Riebe et al., 2017; Grant and Dietrich, 2017; Klos et al., 2018; Rempe and Dietrich, 2018; Dralle et al., 2018; Flinchum et al., 2018; Moravec et al., 2020); and their connection to the nearsurface through the transport of those weathering products to streamflow (Chorover et al., 2017; Kim et al., 2017; McIntosh et al., 2017; Olshansky et al., 2018; White et al., 2019) are crucial to trace weathering reactions and, thus, quantify groundwater contribution from the deep CZ to surface flow. Chemical weathering studies tracing streamflow sources often rely on geochemical and isotopic distinctions of water sources, or end members, to estimate mixing of those sources and to infer water chemistry evolution and flow paths following Hooper et al. (1990). Chemical weathering tracers like major ion chemistry, rare earth elements, and strontium isotopes have long been used (Appelo and Postma, 2005); however, U-series isotopes have emerged more recently as a tracer of chemical weathering and have been suggested to be a reliable tool in studies of groundwater contribution to streamflow and exchange between aquifers (Riotte and Chabaux, 1999; Chabaux et al., 2003, 2008 and references therein; Huckle et al., 2016; Malov, 2018).

A. White et al.

Uranium-series ratios are reported as activity ratios, which are denoted by parentheses herein (e.g. $(^{234}\text{U}/^{238}\text{U})$, $(^{230}\text{Th}/^{238}\text{U})$, etc.) to account for the decay rate, or activity of each U-series isotope wherein activity is calculated as the product of isotope concentration and the decay constant of each respective isotope. The radionuclides of interest in this system are the parent nuclide 238 U ($t_{1/2} = 4.49 \times 10^9$ years) and daughter products of the U-series decay chain, 234 U ($t_{1/2} = 2.48 \times 10^5$ years) and 230 Th ($t_{1/2} = 7.5 \times 10^4$ years) (half-lives from Osmond and Cowart, 1976). Elemental 232 Th ($t_{1/2} = 1.4 \times 10^{10}$ years), which is the parent of another decay series separate from the ²³⁸U-series decay chain, is also used herein to evaluate U and Th mobility. The disequilibrium of U-series isotopes, e.g., excess or deficiencies relative to the parent nuclide ²³⁸U, depends on the decay process, the size of the U-bearing mineral grain, and the distribution of parent ²³⁸U in the vicinity of rockwater interfaces, as well as duration and intensity of water-rock interactions (Chabaux et al., 2008; Porcelli, 2008). For example, U-series isotope fractionation occurs from different behavior of U and Th during alpha recoil and weathering (Chabaux et al., 2003). Alpha recoil is the most common mechanism responsible for disequilibrium between Useries isotopes in water as the crystal lattice of the U-bearing mineral can be damaged during alpha recoil leading to ejection of the short-lived isotope ²³⁴Th (which quickly decays into ²³⁴U) or preferential release of ²³⁴U from the damaged U-bearing mineral during water-rock interaction. Therefore, U-series analysis of solids informs the fractionation processes that occurred over the past ca. 1.25 Ma, after which secular equilibrium (activity of daughter isotope equal to that of parent isotope) is reached.

Aqueous phase U-series activity ratios, particularly ($^{234}\mathrm{U}/^{238}\mathrm{U}$), are gaining popularity as tracers of water-rock interaction. They have commonly been used at large scales to investigate the control of different lithologies on elemental fluxes (Riotte and Chabaux, 1999) or to assess groundwater contributions from regional aquifers to surface flow, the latter because of clear differences in surface and groundwater U-series signatures (Chabaux et al., 2008 and references therein; Bagard et al., 2011). In addition, a large range of U-series values has been observed across aquifers as some studies have found groundwater with very high $(^{234}\text{U}/^{238}\text{U})$ activity ratios (~16; Banner and Hanson, 1990) while several others have found much lower $(^{234}\text{U}/^{238}\text{U})$ activity ratios of groundwater (< 1; Chabaux et al., 2003 and references therein). U-series activity ratios in groundwater, hence, are sensitive to conditions of water-rock interactions and water residence time and flow paths. When different groundwater stores have clearly distinct U-series activity ratios, recent studies have shown that U-series isotopes can be effective tracers of groundwater mixing (Andersson et al., 1995, 1998; Porcelli et al., 1997, 2001; Paces and Wurster, 2014; Huckle et al., 2016;

Navarro-Martinez et al., 2017; Malov, 2018; Rovan et al., 2020).

In cases when U-series activity ratios of groundwater are not distinct, coupling long-studied radiogenic strontium isotope ratios (i.e. ⁸⁷Sr/⁸⁶Sr) with U-series activity ratios can strengthen analysis of groundwater sources to streamflow and inferences about hydrologic flow paths (Roback et al., 2001; Maher et al., 2004; Bagard et al., 2011; Paces and Wurster, 2014; Garcia et al., 2020; Neymark et al., 2018; Beisner et al., 2020; Gardiner et al., 2020). Strontium occurs in trace amounts in most rock types as four stable isotopes (⁸⁴Sr, ⁸⁶Sr, ⁸⁷Sr, and ⁸⁸Sr). Radiogenic Sr isotopes refer to the ratio of ⁸⁷Sr and ⁸⁶Sr isotopes because ⁸⁷Sr is the product of the beta decay of its radiogenic parent nuclide, ⁸⁷Rb. Therefore, the ⁸⁷Sr/⁸⁶Sr composition of rocks depends on its original Rb/Sr ratio and age. Furthermore, waters acquire ⁸⁷Sr/⁸⁶Sr values from water-rock interaction without isotope fractionation and it is often observed that ⁸⁷Sr/⁸⁶Sr values are not in equilibrium with the bulk rock but rather influenced by the most soluble minerals because of incongruent rock dissolution (Roback et al., 2001; Shand et al., 2009). While Sr concentrations are influenced by evaporation, adsorption, or precipitation, ⁸⁷Sr/⁸⁶Sr values are not affected by these processes and are known to be conservative tracers of mineral weathering (Paces et al., 2002; Shand et al., 2009; Porter, 2012; Paces and Wurster, 2014). Recent studies combining the radiogenic isotopic systems of U-series and Sr isotopes have shown their synergistic utility in isotope mixing analysis (Paces and Wurster, 2014; Neymark et al., 2018; Gardiner et al.,

A recent drilling campaign in a small, high elevation zero order basin (ZOB) of the Jemez River Basin Critical Zone Observatory (JRB-CZO) probed the deep CZ and enabled U-series and radiogenic Sr isotope analysis of groundwater and collocated solids from intact continuous cores and multi-level monitoring wells installed in two hillslopes in a small, intensively studied ZOB nested within a larger headwater catchment (La Jara). The paired analysis of collocated groundwater and core samples collected from similar depths below ground surface is a unique contribution to the investigation of water-rock interaction controls on Useries and Sr isotopes. When combined with detailed analysis of the mineralogy and physical structure of the subsurface from past studies (White et al., 2019; Moravec et al., 2020), U-series and Sr isotopes elucidate weathering processes in the deep CZ and mineralogical controls of U-series isotopes. We hypothesize that U-series and Sr isotope profiles in hillslopes with contrasting lithology are controlled by shallow groundwater that facilitates the transport of U and Th, and distinct mineralogy that influences the distribution of U, Th, and Sr with depth due to different weathering processes across hillslopes. Furthermore, combined with U-series and Sr isotope analysis of surface water draining the catchments, detailed analysis of spatial (cores and waters) and temporal (waters) variation in isotope ratios in this small natural setting (ZOB; 0.15 km²) are utilized to estimate groundwater contribution to surface flows at larger scale (La Jara; 3.67 km²). We hypothesize that, together, U-series and Sr isotopes can identify variations in water routing and streamflow contribution in space and across seasons as inputs from shallow and deep groundwater vary as a function of precipitation input and timing. This paper aims to determine how variable mineralogy and structure in the subsurface control the U-series activity ratios and Sr isotope values across depth in the CZ; and then use these isotope tracers to better constrain groundwater contribution to streamflow.

2. Methods

2.1. Study site

The JRB-CZO is situated in the Valles Caldera National Preserve (VCNP) of northern New Mexico (Fig. 1A). The Valles Caldera formed from the collapse of a magma chamber approximately 1.25 Ma ago and eruptions have been documented as recently as 40 ka ago (Wolff et al., 2011). The complex volcanic history of the area created a highly

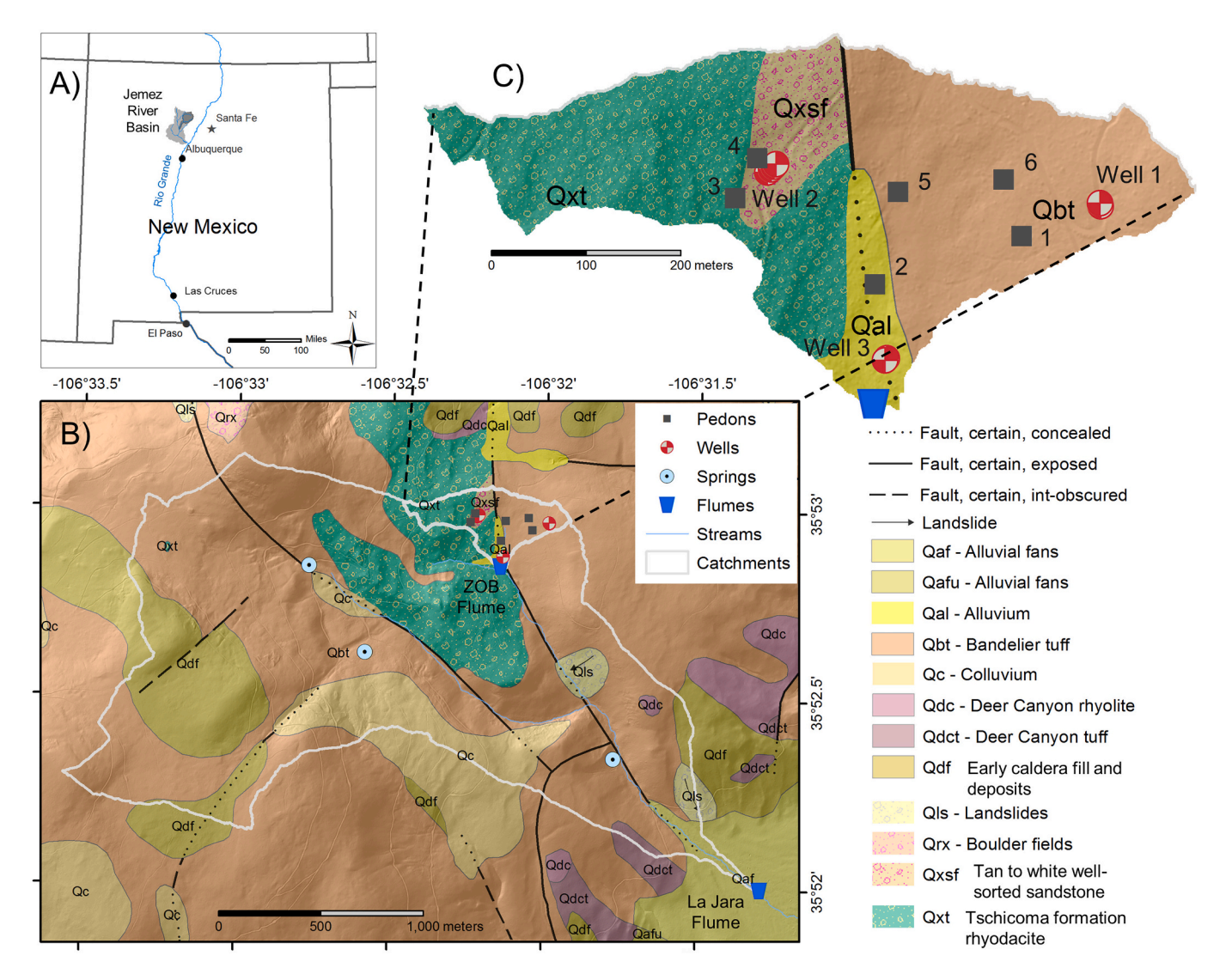


Fig. 1. A) Site map showing the location of the Jemez River Basin Critical Zone Observatory (JRB-CZO) in northern New Mexico in the Valles Caldera National Preserve. B) Site map displaying the catchment outlines of La Jara catchment and the Zero Order Basin (ZOB) within it, along with the location of nested groundwater monitoring wells and surface water flumes within the ZOB and La Jara catchment. C) Inset of the ZOB highlighting locations of instrumented soil pedons and nested groundwater monitoring wells and contrasting rock type of each well site (Site 1 in Bandelier Tuff (Qbt) and Site 2 in volcanic breccia (mapped as caldera-collapse breccia denoted by rock types beginning with "Qx" incorporating sandstone (Qxsf) and rhyodacite (Qxt)). Sampling locations are shown over the geologic map of the area from Goff et al. (2011).

heterogeneous geology throughout the site that has been studied in great detail (Goff et al., 2011; Wolff et al., 2011; Moravec et al., 2020). Redondo Peak, the tallest mountain within the VCNP at an elevation of 3432 masl, consists primarily of Pleistocene partially welded Bandelier Tuff, specifically the Tshriege member, volcanic breccia (mapped as caldera-collapse breccia denoted by rock types beginning with Qx; Fig. 1), and rhyolite (Goff et al., 2011). Soils on Redondo Peak were derived from a mixture of bedrock, ash, and atmospheric dust and consist of well drained Andisols, Alfisols, Mollisols, and Inceptisols (Muldavin and Tonne, 2003a, 2003b).

Temperatures of the sub-humid to semi-arid site average -1 °C in winter and 11 °C in summer (Zapata-Rios et al., 2015). Snow accounts for approximately half of the annual precipitation while the remainder of precipitation falls as rain during the summer monsoon season (Gustafson et al., 2010) generating a bi-modal precipitation pattern in stream discharge (Zapata-Rios et al., 2015; White et al., 2019). La Jara catchment (3.67 km²; Fig. 1B) drains the eastern side of Redondo from elevations of 3429 to 2702 masl with a slope of 15.7° (Perdrial et al., 2014). La Jara creek is a perennial stream gauged at 2739 masl that flows into

the East Fork of the Jemez River, a tributary of the Rio Grande River. A small, gauged headwater catchment (0.15 km²) referred to as the Mixed Conifer Zero Order Basin (ZOB from hereon) is nested within La Jara catchment. Surface flow discharge from the ZOB (flume at 2996 masl) is ephemeral and persists only during spring snowmelt with occasional pulsed flows following summer monsoons and fall storms. In two sites within the ZOB consisting of different rock type (Site 1 in Bandelier Tuff and Site 2 in volcanic breccia; Fig. 1C), nested monitoring wells ranging in total depths from 6.7 to 47.2 m below ground surface (bgs) access groundwater from six depths (White et al., 2019). White et al. (2019) identified distinct groundwater stores across depth and between sites using age dating and major ion chemistry from each monitoring well. The ZOB and greater La Jara catchment are heavily instrumented and have been intensively studied as part of the JRB-CZO, making this site ideal for the small-scale analysis of solid cores and water from two hillslopes with contrasting lithology and the expansion of that analysis to water in the greater catchment.

2.2. Sample preparation and analysis of solid samples

During drilling of groundwater monitoring wells in the ZOB in the summer of 2016, intact continuous cores were collected in plastic sleeves. Cores were cut into subsamples in the field and vacuum sealed in aluminized mylar bags. Select subsamples were air-dried and bulk samples were crushed using a steel mortar and pestle until grain size was less than 250 μm . Crushed samples were then ground to less than 100 μm using a ZrO $_2$ ceramic ball mill. U-series and Sr isotopic analysis of milled samples was conducted at the Center for Earth and Environmental Isotope Research (CEEIR) at the University of Texas at El Paso.

For U-series analysis, sample powders were spiked with an artificial $^{233}\text{U}-^{229}\text{Th}$ tracer and spiked samples were fully digested using HNO₃-HF and HClO₄. U and Th separation and purification was conducted using traditional ion exchange columns (Granet et al., 2007; Pelt et al., 2008; Ma et al., 2010). Concentrations and isotopic ratios of purified samples were analyzed on a Nu Plasma Multicollector Inductively Coupled Plasma Mass Spectrometer (MC-ICPMS, Nu Instruments Ltd., Wrexham, UK). Mass discrimination and ion counter/faraday cup drift during measurements was corrected by bracketing samples with known standard NBL 145B. USGS rock reference standard BCR-2 was also analyzed with samples for quality assurance and the mean BCR-2 $(^{234}\text{U}/^{238}\text{U})$ activity ratio across all runs (n=17) was 1.010 \pm 0.005 (accepted $(^{234}\text{U}/^{238}\text{U})$ activity ratio of 1.000).

For radiogenic Sr analysis, sample powders were fully digested using HNO₃-HF and HClO₄. Sr was separated from the sample matrix with column chemistry using Eichrom® Sr resin following the methods of Konter and Storm (2014). Sr isotopic ratios of purified samples were analyzed on the Nu Plasma MC-ICPMS using the traditional standard sample bracketing method with the known Sr standard NIST SRM 987. USGS rock reference standard BCR-2 (accepted $^{87}{\rm Sr}/^{86}{\rm Sr}$ of 0.70502) was also analyzed with each run for quality assurance and the average BCR-2 $^{87}{\rm Sr}/^{86}{\rm Sr}$ value was 0.70502 \pm 0.00002 (n=25).

2.3. Water sample collection and sample analysis

Surface water samples from the ZOB and La Jara creek were collected as grab samples at flume locations (Fig. 1B) throughout 2017 and part of 2018. Surface water samples were collected biweekly except during times of snow cover when access to the sites was limited. Groundwater samples were collected using a Waterra inertial pump (Waterra USA Inc., Peshatin, WA, USA), Geotech SS Geosub Pump (Geotech Environmental Equipment, Inc., Denver, CO, USA), 42.1 mm stainless-steel bailer (Geotech Environmental Equipment, Inc., Denver, CO, USA), or ISCO autosampler (Teledyne, ISCO, NE, USA; at well 2D only) depending on time of year, site access, and monitoring well dimensions. See White et al. (2019) for further details of groundwater monitoring wells such as screened interval depths, groundwater sampling methods, and sampling frequency.

All water samples were collected in DI-washed and combusted amber glass bottles (for carbon) and acid-washed polypropylene bottles (for cations, U-series, and Sr isotope analysis). All bottles were triple rinsed with sample water prior to sample collection and samples were kept cold until prompt filtration at the University of Arizona. Carbon sample splits were filtered through 0.7 µm glass fiber filters while cation and isotope sample splits were filtered through 0.45 µm nylon filters and acidified with trace metal grade HNO3. Dissolved organic carbon (DOC) and dissolved inorganic carbon (DIC) were measured using a Shimadzu TOC-VCSH analyzer (Shimadzu Scientific Instruments, Columbia, MD, United States) and cations were analyzed on an ICP-MS equipped with a collision cell to eliminate isobaric influences (Agilent 7700X, Santa Clara, CA, United States) at the University of Arizona Laboratory for Emerging Contaminants (ALEC). Further sample preparation (i.e. U and Sr purification via column chemistry) and analysis of U-series and radiogenic Sr isotopes on Nu MC-ICPMS were conducted at CEEIR at the University of Texas at El Paso. Saturation indices with respect to calcite were

calculated using PHREEQC with temperature, pH, and DIC concentrations as inputs.

Uranium was concentrated by evaporating water samples to obtain approximately 50 ng of U for analysis. Uranium was purified and isolated from sample matrix using ion exchange column chemistry similar to that outlined above in Section 2.2. Purified samples were analyzed for U-series isotope ratios on a Nu MC-ICPMS. Uranium standard NBL 145B was used for standard bracketing and the USGS rock reference standard BCR-2 was also analyzed with samples for quality assurance, with mean $(^{234}\mathrm{U}/^{238}\mathrm{U})$ activity ratio $=1.010\pm0.005$ (n=17).

Strontium was concentrated by evaporating filtered and acidified samples to obtain Sr concentrations of approximately 1 μ g of Sr. Strontium was then isolated from sample matrix using ion exchange columns filled with Eichrom® Sr resin as explained in Section 2.2. Purified Sr samples were analyzed on the Nu MC-ICPMS for isotope ratios. For quality assurance, the USGS rock reference standard BCR-2 was analyzed, with average BCR-2 87 Sr/ 86 Sr = 0.70502 \pm 0.00002 (n = 25).

3. Results

3.1. Weathering profiles of solid cores

Mobility behaviors of U-series isotopes (²³⁸U, ²³⁴U, and ²³⁰Th), such as U addition or release from weathering, and production and decay of ²³⁴U and ²³⁰Th from their parent nuclide, ²³⁸U, are evaluated in bivariate plots of (²³⁴U/²³⁸U) and (²³⁰Th/²³⁸U) activity ratios (Thiel et al., 1983; Osmond and Ivanovich, 1992; Dequincey et al., 2002; Chabaux et al., 2003; Ma et al., 2010). $(^{234}\text{U}/^{238}\text{U})$ activity ratios of bulk samples of Site 1 core are near secular equilibrium with a small range from 0.966 to 1.045 while (230 Th/ 238 U) activity ratios remain less than, but close to secular equilibrium with a range from 0.847 to 0.988 (Table 1). All bulk samples of Site 1 core are tightly grouped around secular equilibrium of $(^{234}\text{U}/^{238}\text{U})$ and $(^{230}\text{Th}/^{238}\text{U})$ activity ratios spanning the top and bottom left quadrants of the (²³⁴U/²³⁸U) versus (²³⁰Th/²³⁸U) cross plot (Fig. 2A). In contrast, Site 2 core samples are farther from secular equilibrium and exhibit greater disequilibrium of (230Th/238U) and $(^{234}\text{U}/^{238}\text{U})$ activity ratios. $(^{234}\text{U}/^{238}\text{U})$ activity ratios of Site 2 core samples range from 0.759 to 1.158, while (230Th/238U) activity ratios range from 0.871 to 1.280 (Table 1). Site 2 core samples plot primarily in the bottom left and top right quadrants of the $(^{230}\text{Th}/^{238}\text{U})$ versus $(^{234}\text{U}/^{238}\text{U})$ cross plot (Fig. 2A) with one sample plotting in the bottom right quadrant.

Ratios of $^{238}\rm U$ and $^{230}\rm Th$ normalized to $^{232}\rm Th$ of core samples from Sites 1 and 2 are shown in reference to the deepest core of each respective site (Fig. 2B) to evaluate U and Th mobility with depth. $(^{238}\rm U/^{232}\rm Th)$ activity ratios of Site 1 core samples range from 0.318 to 0.849 and $(^{230}\rm Th/^{232}\rm Th)$ activity ratios range from 0.301 to 0.791 (Table 1). Some Site 1 samples have greater $(^{238}\rm U/^{232}\rm Th)$ and $(^{230}\rm Th/^{232}\rm Th)$ activity ratios than the deepest Site 1 core sample while others have lower $(^{238}\rm U/^{232}\rm Th)$ and $(^{230}\rm Th/^{232}\rm Th)$ activity ratios than the deepest Site 1 core sample. In contrast, all but one Site 2 core sample have higher $(^{238}\rm U/^{232}\rm Th)$ and $(^{230}\rm Th/^{232}\rm Th)$ activity ratios than the deepest Site 2 core sample. Site 1 core samples plot more tightly along the equiline than Site 2 core samples (Fig. 2B).

Bulk core samples display clear variations in U-series activity ratios and U concentrations with depth (Table 1); however, it is important to note the significantly greater variability in (234 U/ 238 U) activity ratios at Site 2 compared to Site 1 (Fig. 3). (234 U/ 238 U) and (230 Th/ 238 U) activity ratios of Site 1 core show limited variability with depth. (234 U/ 238 U) activity ratios of Site 2 core samples are significantly depleted in 234 U within the top 3 mbgs ((234 U/ 238 U) activity ratios range from 0.938 to 0.903), greatly depleted at 3.5 mbgs ((234 U/ 238 U) activity ratio of 0.759), fairly near secular equilibrium at approximately 16 mbgs ((234 U/ 238 U) activity ratio of 0.980), considerably enriched in 234 U at approximately 21 mbgs ((234 U/ 238 U) activity ratio of 1.158), and slightly less than secular equilibrium at maximum depth of

Table 1
Radiogenic Sr isotope and U-Series activity ratios and elemental concentrations of Sr and U for core samples from Sites 1 (top) and 2 (bottom). Reported errors (2σ) are internal precision of single measurements.

Site 1													
Depth (mbgs)	Zone	⁸⁷ Sr/ ⁸⁶ Sr	$\pm~2\sigma$	Sr (mg/ kg)	(²³⁴ U/ ²³⁸ U)	$\pm~2\sigma$	(²³⁰ Th/ ²³⁸ U)	$\pm~2\sigma$	(²³⁰ Th/ ²³² Th)	$\pm~2\sigma$	(²³⁸ U/ ²³² Th)	$\pm~2\sigma$	U (mg/ kg)
1.1	Soil/ Saprolite	0.70564	0.00006	73.8	0.986	0.005	0.946	0.009	0.732	0.007	0.774	0.009	2.20
1.8	Soil/ Saprolite	0.70598	0.00003	81.5	0.966	0.005	0.911	0.009	0.612	0.006	0.672	0.008	2.05
4.2	Soil/ Saprolite	0.70698	0.00002	496	1.000	0.005	0.944	0.009	0.301	0.003	0.318	0.004	1.03
4.6	Soil/ Saprolite	-	-	-	0.982	0.005	0.847	0.008	0.361	0.004	0.426	0.005	1.40
12.8	Transition Zone	0.70611	0.00005	52.7	1.045	0.005	0.962	0.010	0.680	0.007	0.706	0.008	2.00
20.5	Tuff	_	_	_	1.014	0.005	0.949	0.009	0.672	0.007	0.708	0.008	2.06
28.1	Tuff	0.70589	0.00008	57.4	0.993	0.005	0.932	0.009	0.791	0.008	0.849	0.010	2.71
35.6	Tuff	0.70550	0.00002	57.5	0.976	0.005	0.948	0.009	0.535	0.005	0.564	0.007	1.64
41.7	Tuff	0.70555	0.00003	57.5	1.010	0.005	0.988	0.010	0.722	0.007	0.731	0.009	2.06
Site 2													
Depth (mbgs)	Zone	⁸⁷ Sr/ ⁸⁶ Sr	$\pm \ 2\sigma$	Sr (mg/ kg)	(²³⁴ U/ ²³⁸ U)	$\pm \ 2\sigma$	(²³⁰ Th/ ²³⁸ U)	$\pm~2\sigma$	(²³⁰ Th/ ²³² Th)	$\pm~2\sigma$	(²³⁸ U/ ²³² Th)	$\pm \ 2\sigma$	U (mg kg)
1.1	Soil/ Saprolite	0.71397	0.00006	124	0.938	0.005	0.912	0.009	0.951	0.010	1.042	0.013	3.45
2.6	Breccia	0.72334	0.00002	146	0.903	0.005	0.890	0.009	0.871	0.009	0.978	0.012	1.35
3.5	Breccia	0.71834	0.00004	105	0.759	0.004	0.817	0.008	1.101	0.011	1.347	0.016	2.86
6.7	Tuff Boulder	0.70697	0.00002	24.7	0.972	0.005	0.909	0.009	0.952	0.010	1.046	0.013	6.48
15.8	Ash	0.70766	0.00002	557	0.980	0.005	1.029	0.010	0.365	0.004	0.354	0.004	1.02
21.0	Vesicular Tuff	0.70652	0.00002	106	1.158	0.006	1.645	0.016	1.280	0.013	0.778	0.009	2.13
35.7	Vesicular Tuff	0.70588	0.00003	111	1.112	0.006	1.064	0.011	0.814	0.008	0.766	0.009	2.45
44.8	Vesicular Tuff	0.70541	0.00005	41.7	0.960	0.005	0.942	0.009	0.568	0.006	0.603	0.007	2.05

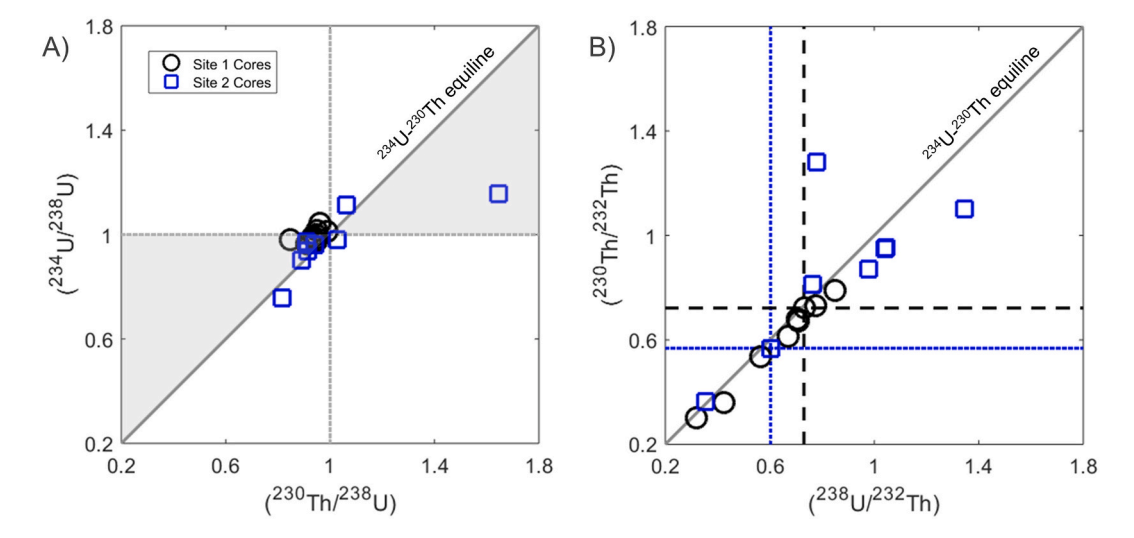


Fig. 2. U-series activity ratios from Site 1 and 2 core samples. $^{234}U^{-230}Th$ equilines are shown on both plots and error (2σ) for each sample measurement is smaller than the marker size. Secular equilibrium is shown as a dotted gray line at activity ratio of 1 for the left plot of $(^{234}U/^{238}U)$ and $(^{230}Th/^{238}U)$ activity ratios (A) and the shaded regions show "complex zones" of weathering (Dequincey et al., 2002). The black dashed lines on the right plot of $(^{230}Th/^{232}Th)$ and $(^{238}U/^{232}Th)$ activity ratios (B) mark the respective activity ratios of the deepest Site 1 core and the blue dotted lines on the right plot mark the activity ratios of the deepest Site 2 core. (For interpretation of the references to colour in this figure legend, the reader is referred to the web version of this article.)

approximately 45 mbgs ((234 U/ 238 U) activity ratio of 0.960). At Site 2, the shape of (234 U/ 238 U) and (230 Th/ 238 U) activity ratio depth trends are similar to one another (Fig. 2A); however, the enrichment of 230 Th at approximately 21 mbgs is greater than the enrichment of 234 U at that

same depth (Fig. 3A and B). Furthermore, the (234 U/ 238 U) activity ratio of the shallowest core sample at each site agrees with (234 U/ 238 U) activity ratios of previously measured ZOB soils (Huckle et al., 2016; Fig. 3A). (238 U/ 232 Th) activity ratios of Site 1 core samples display

A. White et al. Chemical Geology 570 (2021) 120156

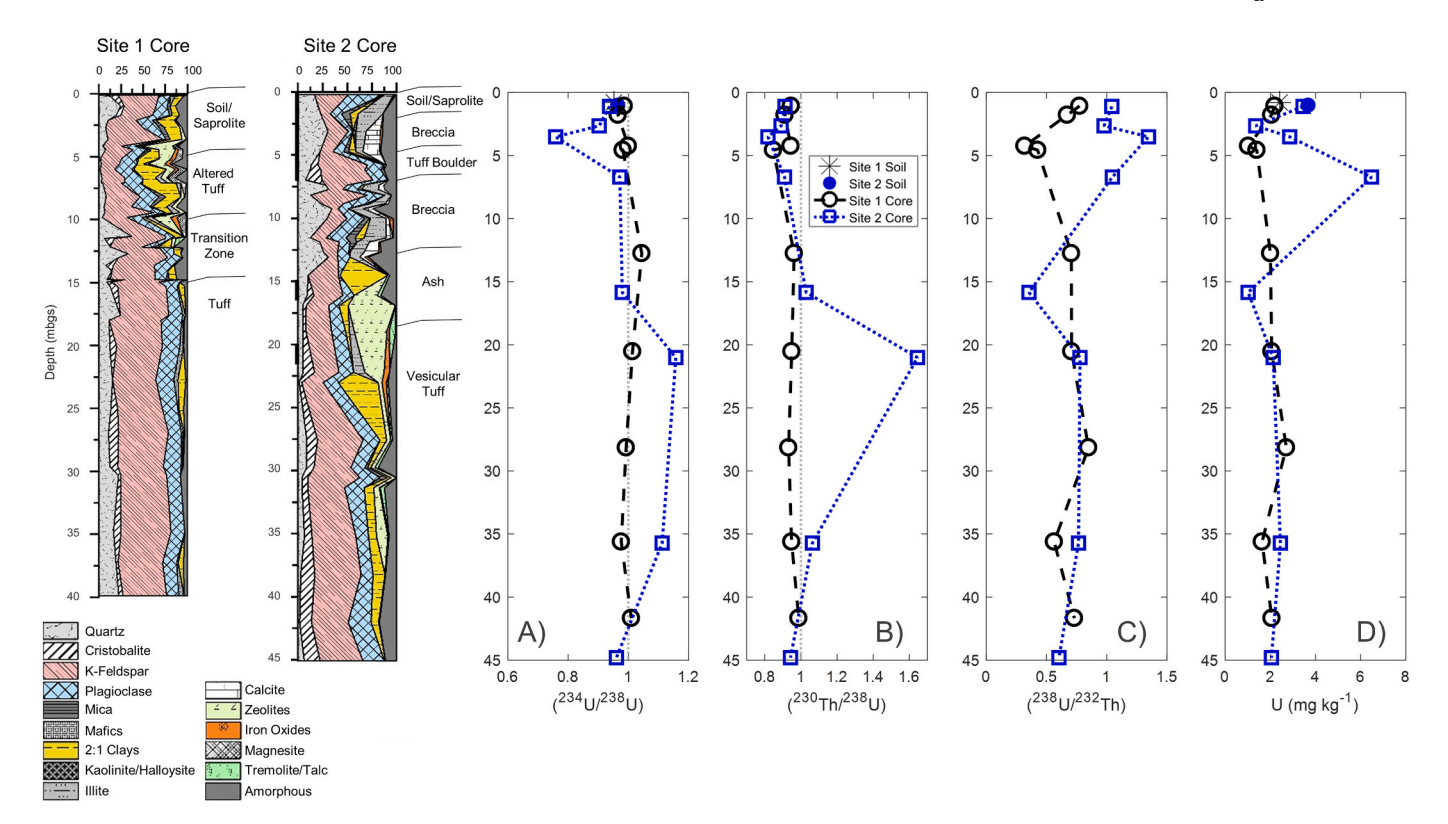


Fig. 3. Quantitative mineralogy and lithology modified from Moravec et al. (2020) and U-series activity ratios from Site 1 and 2 core samples across depth. Secular equilibrium is shown as a dotted gray line at activity ratio of 1 for A) (234 U/ 238 U) activity ratios and B) (230 Th/ 238 U) activity ratios, but not for C) (238 U/ 232 Th) activity ratios or D) U concentration. Error bars (20) for each sample are smaller than the marker size. Soil data are from Huckle et al. (2016).

greater variability, but similar depth trends as those of $(^{234}\text{U}/^{238}\text{U})$ and $(^{230}\text{Th}/^{238}\text{U})$ activity ratios whereas $(^{238}\text{U}/^{232}\text{Th})$ activity ratios of Site 2 cores exhibit different trends than the other Site 2 activity ratios with more U than Th in the near surface and less U than Th at approximately 16 mbgs (Fig. 3C).

⁸⁷Sr/⁸⁶Sr values also vary with depth in Site 1 and 2 cores (Table 1; Fig. 4A). In Site 1 core samples, there is a slight increase in ⁸⁷Sr/⁸⁶Sr values towards a more radiogenic signature just above 5 mbgs (0.70698). Beneath that, ⁸⁷Sr/⁸⁶Sr values vary very little and trend towards the deepest core signature of 0.70555. Solid cores from Site 2 have a far greater radiogenic signature (0.71834 at approximately 3.5 mbgs) than those seen in Site 1 core samples. Site 2 core samples also display a more radiogenic signature at approximately 16 mbgs compared to the ⁸⁷Sr/⁸⁶Sr signature at depth. Beneath 16 mbgs, Site 2 core samples also trend towards lower ⁸⁷Sr/⁸⁶Sr values like that of the deepest Site 2 core (0.70541; Table 1). Furthermore, the ⁸⁷Sr/⁸⁶Sr signature at the greatest depth of core from Sites 1 and 2 is similar.

In Site 1 core, Sr concentrations increase up to 496 mg/kg in the top 5 mbgs, and beneath approximately 12 mbgs Sr concentrations decrease and remain within a tight range of 53 to $58 \, mg/kg$ to the greatest depths of sampled core. In contrast, elemental Sr concentrations of Site 2 are more variable than those of Site 1 core samples and closely resemble the Site 2 depth profile of ⁸⁷Sr/⁸⁶Sr values with peaks in Sr concentration of 105 and 557 mg/kg at 3 and 16 mbgs, respectively (Fig. 4A and B). In addition, the ⁸⁷Sr/⁸⁶Sr values and Sr concentrations of near surface Site 2 core samples coincide with soils previously collected near the Site 2 wells (Porter, 2012; pedons 3 and 4 in Fig. 1B and C), in contrast to Site 1 where 87Sr/86Sr values of Site 1 near surface core samples are much lower than those of soils collected from pedons 1 and 6 near the Site 1 wells (Porter, 2012; Fig. 1B and C). Furthermore, Sr concentrations of core samples within the top 5 mbgs at Site 1 are higher than those of soils while Sr concentrations of core samples at greater depth are consistent with the soils (Fig. 4A and B).

3.2. Water-rock interactions: Solid and solution samples

Comparison of $(^{234}\text{U}/^{238}\text{U})$ activity ratios in solid cores and collocated groundwaters can constrain controls of water-rock interactions on U-series activity ratios. As expected, all $(^{234}\text{U}/^{238}\text{U})$ activity ratios of groundwater are greater than secular equilibrium (Table 2). $(^{234}\text{U}/^{238}\text{U})$ activity ratios of groundwater from well 1A range from 1.588 to 2.018 (mean of 1.691, n=10) and overlap with the range of groundwater from well 1B $(^{234}\text{U}/^{238}\text{U})$ activity ratios from 1.741 to 2.065 with a mean activity ratio of 1.888 (n=9) (Fig. 5A). At the depth nearest the Site 1 water table (~35 mbgs), Site 1 core samples are slightly depleted in ^{234}U and have an $(^{234}\text{U}/^{238}\text{U})$ activity ratio of 0.976 (Fig. 5A). As indicated in Section 3.1, all Site 1 solid core samples show limited variation in $(^{234}\text{U}/^{238}\text{U})$ activity ratios ranging from 0.966 to 1.045 (Table 1).

Individual groundwater stores at Site 2 have distinct $(^{234}\text{U}/^{238}\text{U})$ activity ratios (Table 2). Shallow groundwater from well 2D has the highest values and largest range of $(^{234}\text{U}/^{238}\text{U})$ activity ratios (2.527 to 2.971 with a mean ($^{234}\text{U}/^{238}\text{U}$) activity ratio of 2.791, n = 10). The most depleted (234 U/ 238 U) activity ratio of Site 2 solid core samples (0.759) comes from approximately 3.5 mbgs, within the range of the well 2D water table depth (Fig. 5B). (²³⁴U/²³⁸U) activity ratios of groundwater from well 2C (~28 mbgs) range from 2.488 to 2.720 with a mean value of 2.612 (n = 9) while the Site 2 core ($^{234}U/^{238}U$) activity ratio nearest the depth of well 2C groundwater is 1.112 (Fig. 5B). Deeper groundwater from well 2B (~38 mbgs) has an activity ratio of 2.084 and Site 2 core nearest that depth has an activity ratio of 1.112 (Fig. 5B). $(^{234}\text{U}/^{238}\text{U})$ activity ratios of the deepest groundwater from Site 2 (well 2A at \sim 45 mbgs) has (234 U/ 238 U) activity ratios ranging from 2.245 to 2.340 with an average of 2.293 (n = 2) that corresponds to a Site 2 core $(^{234}U/^{238}U)$ activity ratio of 0.960 (Fig. 5B).

 $(^{234}\text{U}/^{238}\text{U})$ activity ratios and Log[U] of groundwater stores from Sites 1 and 2 do not show any clear trends (Fig. 6A); however, there is greater variability in $(^{234}\text{U}/^{238}\text{U})$ activity ratios relative to Log[U] of

A. White et al. Chemical Geology 570 (2021) 120156

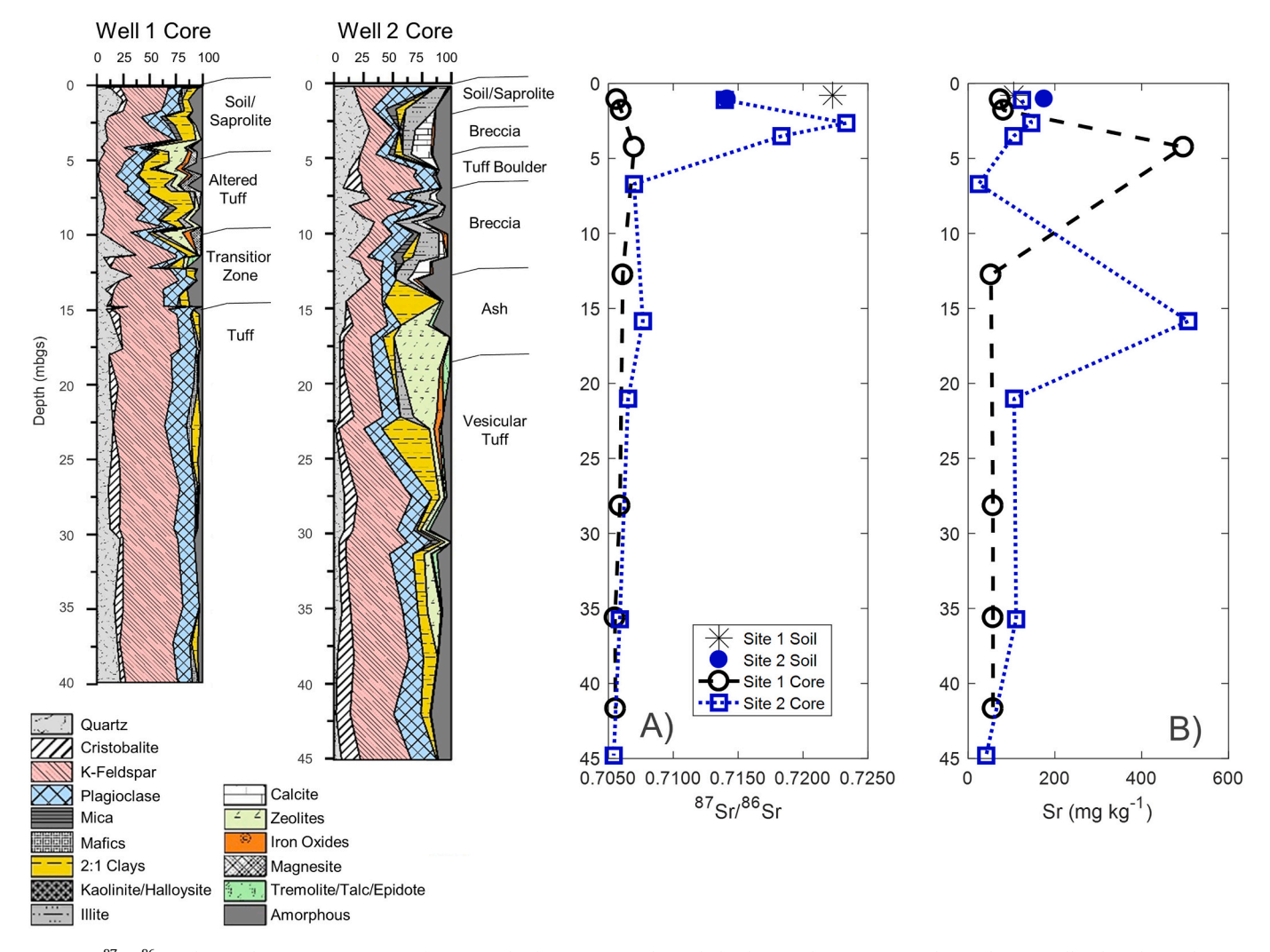


Fig. 4. A) ⁸⁷Sr/⁸⁶Sr values and B) Sr concentration of core samples from Sites 1 and 2 with depth. Error bars (2σ) for each sample are smaller than the marker size. Quantitative mineralogy and lithology of Site 1 and 2 cores modified from Moravec et al. (2020). Sr isotope values and concentrations of soils from Sites 1 and 2 are from Porter (2012).

groundwater from Site 2 while the opposite is true with greater variability in Log[U] than in (234 U/ 238 U) activity ratios of Site 1 groundwater. Furthermore, each groundwater store has a clear and distinct (234 U/ 238 U) activity ratio and Log[U] signature and the signature of ZOB and La Jara surface water is closer to the lower (234 U/ 238 U) activity ratio and Log[U] signature of Site 1 groundwater. In addition, Site 2 groundwater (except one sample from the deepest Site 2 groundwater) is near equilibrium (i.e., saturated) with respect to calcite while Site 1 groundwaters and surface waters from the ZOB and La Jara are undersaturated with respect to calcite (Fig. 7A and B).

Groundwater from Sites 1 and 2 and surface water from La Jara and ZOB streams have somewhat distinct ⁸⁷Sr/⁸⁶Sr values and Sr concentrations (Fig. 6B). Generally, Site 2 groundwater from all depths has higher Sr concentrations than surface water and groundwater from the fractured tuff aquifer at Site 1; however, Sr concentrations of groundwater from well 2C are similar to those of Site 1 groundwater and some La Jara surface water samples. Shallow groundwater from well 2D has the most radiogenic signature and highest Sr concentrations while the deepest groundwater from the fractured tuff aquifer at Site 1 has the lowest ⁸⁷Sr/⁸⁶Sr values. Furthermore, there are no clear relationships between ⁸⁷Sr/⁸⁶Sr values and Sr concentrations in ground or surface water (Fig. 6B).

3.3. Time series of groundwater and surface water

Time series of U-series and Sr isotopes span from March 2017 to February 2018 for groundwater from wells 1A, 1B, 2C, and 2D, February 2017 to February 2018 for La Jara surface water, and March 2017 to August 2017 for ZOB surface water. While $(^{234}U/^{238}U)$ activity ratios and ⁸⁷Sr/⁸⁶Sr values are specific to each groundwater store (Fig. 5 and 6), it is also important to note temporal variability of isotope signatures for each reservoir (Figs. 8 and 9). Generally, there is little difference between 87Sr/86Sr values of each Site 1 groundwater store over time while $(^{234}\text{U}/^{238}\text{U})$ activity ratios of the two groundwater reservoirs in the Site 1 fractured tuff are most similar during baseflow conditions during the winter and diverge across higher flow periods during snowmelt, monsoons, and fall storms. For instance, $(^{234}U/^{238}U)$ activity ratios of groundwater from well 1B are considerably higher than those of well 1A at the end of June 2017 (Fig. 8). Furthermore, $(^{234}\text{U}/^{238}\text{U})$ activity ratios of deep groundwater from the fractured tuff water stores are lowest as the water table recedes following peak heights, coincident with the rise in DOC concentration (an indicator of soil water contributions; Perdrial et al., 2014; Olshansky et al., 2018) in well 1A groundwater.

Site 2 groundwater (234 U/ 238 U) activity ratios are more variable over time as the water table rises and falls and (234 U/ 238 U) activity ratios of groundwater from wells 2D and 2C change simultaneously during fall

Chemical Geology 570 (2021) 120156

Table 2
Radiogenic Sr isotope values, U-series activity ratios, number of samples (n) and mean concentrations of surface (La Jara and ZOB) and groundwater (wells) across the study period. One standard deviation calculated from all samples per type is shown in italics inside of parentheses.

	87 Sr/ 86 Sr	$(^{234}U/^{238}U)$	Sr (ppb)	U (ppb)	Ca (ppm)	DOC (ppm)	DIC (ppm)	pH
La Jara								
	0.70767	1.997	37	0.013	7.0	3.8	3.4	7.08
	(0.00002)	(0.107)	(5.8)	(0.015)	(1.6)	(2.5)	(0.68)	(0.375)
ZOB	n = 9	n = 13	n = 157	n = 158	n = 160	n = 156	n = 160	n=155
ZOB	0.70794	1.694	54	0.042	11	9.1	5.9	6.99
	(0.00023)	(0.057)	(11)	(0.011)	(2.1)	(2.3)	(1.8)	(0.399)
YAY-11 1 A	n = 7	n=7	n = 99	n=99	n = 139	n = 138	n = 140	n=129
Well 1A	0.70741	1.691	60.	0.38	14	3.2	14.4	7.45
	(0.00007)	(0.116)	(12)	(0.50)	(4.2)	(4.0)	(2.7)	(0.370)
W-11 1 D	n = 10	n = 10	n=14	n=14	n=16	n = 17	n = 18	n=16
Well 1B	0.70718	1.888	59	0.26	10.	3.2	10.2	7.30
	(0.00008)	(0.097)	(34)	(0.35)	(5.8)	(3.9)	(3.0)	(0.407)
Well 2A	n = 9	n = 9	n=13	n=13	n=16	n=14	n=16	n=13
Well 2A	0.70728	2.293	180	2.4	40.	3.0	42.1	7.82
	(0.00000)	(0.047)	(31)	(0.53)	(5.2)	(1.8)	(24.6)	(0.154)
Well 2B	n = 2	n = 2	n = 4	n = 4	n=4	n = 3	n = 4	n = 4
Well 2b	0.70743	2.084	160	17	26	7.6	70.5	8.21
			(5.7)	(0.18)	(1.4)			(0.550)
Well 2C	n=1	n=1	n=2	n=2	n=2	n=1	n=1	n=2
Well 2C	0.70756	2.612	77	4.7	87	1.5	56.7	7.59
	(0.00008)	(0.080)	(17)	(1.2)	(19)	(1.9)	(6.7)	(0.171)
W-11 0D	n = 9	n = 9	n=15	n=15	n = 19	n=17	n = 21	n=17
Well 2D	0.70860	2.791	250	1.3	107	2.8	60.9	7.53
	(0.00013)	(0.176)	(50.)	(0.42)	(11)	(0.62)	(6.3)	(0.291)
	n=10	n=10	n = 79	n = 79	n = 81	n = 80	n = 82	n=81

storms. Generally, (²³⁴U/²³⁸U) activity ratios of groundwater from wells 2D and 2C are higher when the shallow groundwater table is lower and lowest when the shallow groundwater table is highest (Fig. 9). ⁸⁷Sr/⁸⁶Sr values of Site 2 groundwater decrease gradually during spring snowmelt, increase slightly throughout summer and fall storms, and decrease again as the shallow groundwater table recedes.

 $(^{234}\mathrm{U}/^{238}\mathrm{U})$ activity ratios of La Jara stream water decrease slightly at the onset of spring snowmelt, increase gradually as streamflow recedes from summer monsoon storms, and return to $(^{234}\mathrm{U}/^{238}\mathrm{U})$ activity ratios of the snowmelt period throughout fall storms and winter baseflow (Figs. 8 and 9). $(^{234}\mathrm{U}/^{238}\mathrm{U})$ activity ratios of ZOB stream water increase slightly from the onset of spring snowmelt through summer monsoons. Coincident with DOC concentrations, $^{87}\mathrm{Sr}/^{86}\mathrm{Sr}$ values of ZOB surface water are consistently high throughout spring snowmelt at more radiogenic values than the $^{87}\mathrm{Sr}/^{86}\mathrm{Sr}$ signature of La Jara surface water and they drop during summer storms, whereas $^{87}\mathrm{Sr}/^{86}\mathrm{Sr}$ values of La Jara surface water decrease very slightly during spring snowmelt, peak during summer storms, and decrease slightly during fall storms.

4. Discussion

4.1. Distribution of U-series and Sr isotopes in cores

We observe stark differences in the fractionation history and weathering intensity of cores at Sites 1 and 2 that we attribute to the different subsurface properties associated with their contrasting lithology, the mineralogical control of zeolites, and the presence and absence

of shallow groundwater at Site 2 and Site 1, respectively. Specifically, Site 2 core samples show scatter away from the ²³⁰Th—²³⁴U equiline (Fig. 2; Harmon and Rosholt, 1982) indicating significant recent (<0.4 Ma) disturbance causing U—Th fractionation to the system (Fig. 2B). The typical signature of U and Th loss from weathering is seen within the top 7 mbgs where ($^{234}\text{U}/^{238}\text{U}$) and ($^{230}\text{Th}/^{238}\text{U}$) activity ratios in Site 2 core samples are less than secular equilibrium with considerable depletion at 3.5 mbgs (Fig. 3), coincident with the depth of the shallow groundwater table. We hypothesize that shallow groundwater facilitates weathering and transports U and Th from the top 7 mbgs, where an intense weathering signature is seen, to depth where it is deposited beneath the ash layer at Site 2, shown by a substantial enrichment in 234 U and 230 Th and elevated (238 U/ 232 Th) activity ratios (Fig. 3). This is corroborated by Site 2 core samples from depths of 21 and 36 mbgs that plot in the upper right quadrant of $(^{234}\text{U}/^{238}\text{U})$ and $(^{230}\text{Th}/^{238}\text{U})$ bivariate plots (Fig. 2A) indicating U addition and subsequent ingrowth of ²³⁰Th. Similar to that seen in a ferrallitic soil in Cameroon (Chabaux et al., 2003) and in a lateritic profile in Burkina Faso (Dequincey et al., 2002), $(^{234}\text{U}/^{238}\text{U})$ and $(^{230}\text{Th}/^{238}\text{U})$ activity ratio trends suggest progressive U movement from the surface down to underlying horizons, in this case down to the top of the vesicular tuff layer (~21 mbgs; Fig. 3) where zeolites are found to occur at approximately 25% by mass and Mn and Fe tau mass transfer values increase, showing enrichment relative to the least weathered portions of the profile (Moravec et al., 2020). Uranium addition to layers with increased zeolite mass fraction suggests that ²³⁴U is brought into the system and decays to ²³⁰Th, which is strongly sorbed to zeolites, and leads to greater ($^{230}\text{Th}/^{238}\text{U}$) activity

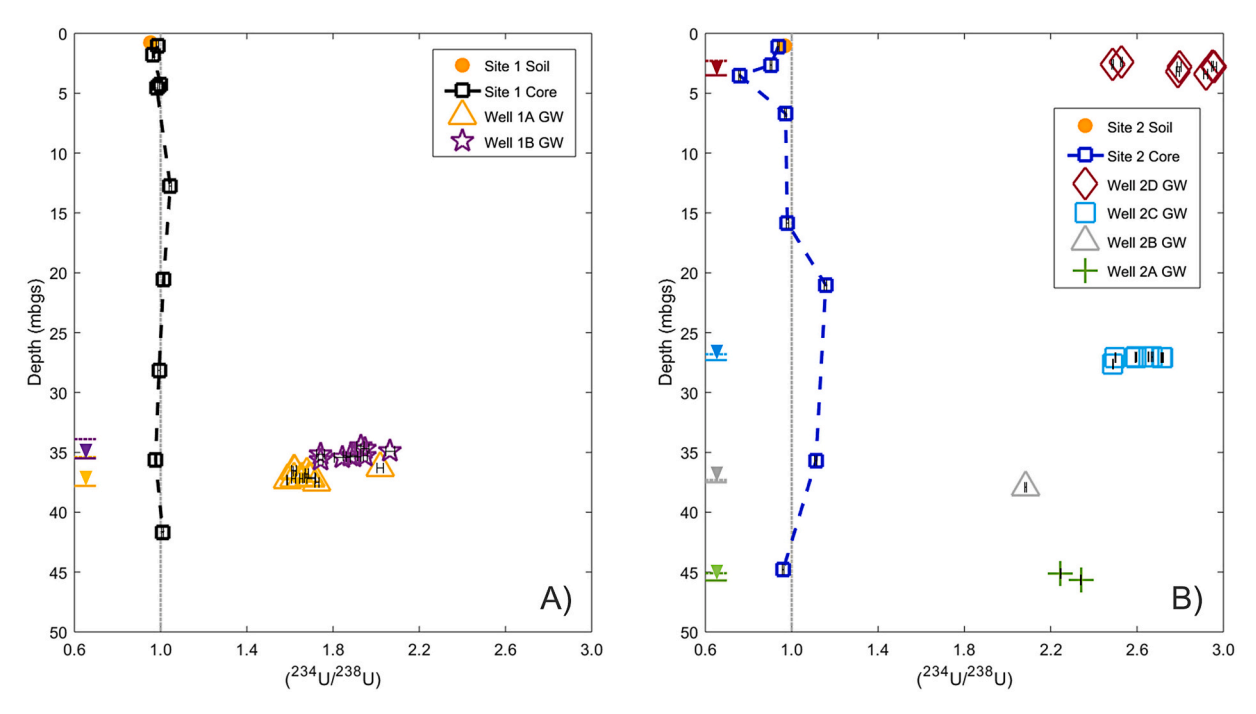


Fig. 5. $(^{234}\text{U}/^{238}\text{U})$ activity ratios of core samples and groundwaters as a function of depth for A) Site 1 and B) Site 2, respective to each site's ground surface elevation (3020 and 3024 masl, respectively). Secular equilibrium is shown as a dotted gray line at an activity ratio of 1. Error bars show internal precision (2 σ) of single measurements. Groundwater depths refer to depth to water table below ground surface (bgs) immediately prior to sampling. The range of water table fluctuation is shown along the y-axis as the difference between water table minimum, denoted as a solid line topped with an inverted triangle, and water table maximum, denoted as a dashed line, in the respective colour for each well. Soil data are from Huckle et al. (2016).

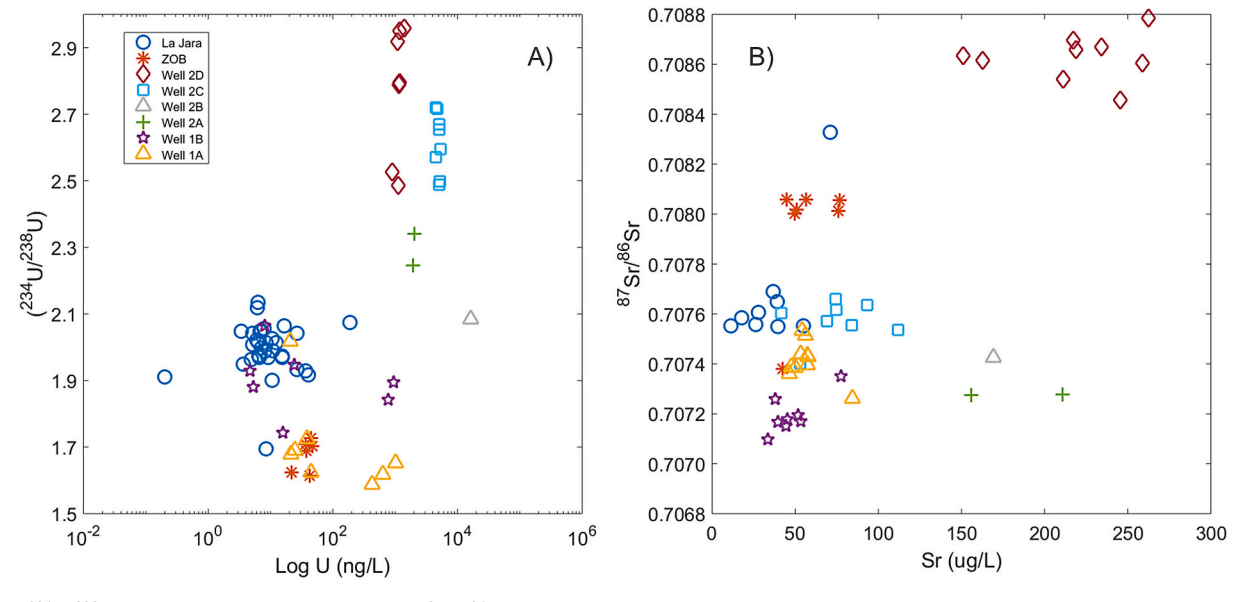


Fig. 6. A) (234 U/ 238 U) activity ratios versus Log[U] and B) 87 Sr/ 86 Sr values versus Sr concentration of groundwater from Sites 1 and 2 and surface water from La Jara creek and ZOB.

ratios compared to $(^{234}U/^{238}U)$ activity ratios.

We also hypothesize that the presence of organic-rich shallow groundwater (Table 2) and subsequent colloids lead to the loss of $^{232}{\rm Th}$ from the depth of the shallow aquifer at Site 2, as Th is known to complex with organic colloids (Viers et al., 1997; Dupré et al., 1999; Porcelli et al., 1997, 2001; Riotte et al., 2003; Bagard et al., 2011). We suggest that in this system, elevated ($^{238}{\rm U}/^{232}{\rm Th}$) activity ratios down to 7 mbgs at Site 2 (Fig. 3) are the result of $^{232}{\rm Th}$ mobilization with colloids that are transported to the ash layer at 16 mbgs at Site 2 where organic colloids begin to break down. While it appears that there are some

qualitative links between U and Th mobility, mineralogy, and lithology, there are no obvious strong relationships between U—Th activity ratios and mineral mass fractions, like zeolites or clays (Supplemental Figs. 1, 2, and 3) or weathering indices (Supplemental Fig. 4), perhaps because of the limited number of core samples.

In contrast, Site 1 core samples plot on or very near the ²³⁰Th—²³⁴U equiline that denotes steady state in bi-variate plots of (²³⁰Th/²³²Th) vs (²³⁸U/²³²Th) (Harmon and Rosholt, 1982), which indicates that (²³⁸U/²³²Th) activity ratio disequilibria occurred greater than 0.4 Ma ago (Dequincey et al., 2002) and is consistent with the limited

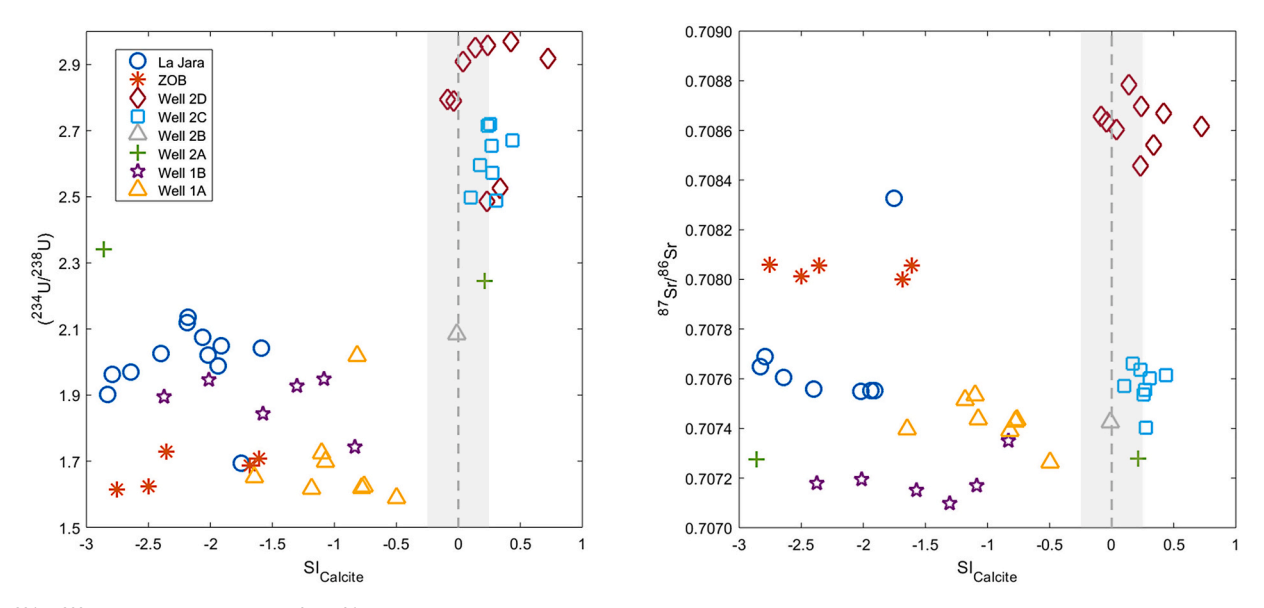


Fig. 7. (234U/238U) activity ratios (A) and 87Sr/86Sr values (B) versus calcite saturation index of groundwater stores from Sites 1 and 2 and surface water from La Jara creek and ZOB flumes. An error of 2.5% (shaded gray region) is shown around equilibrium according to Szramek et al. (2007).

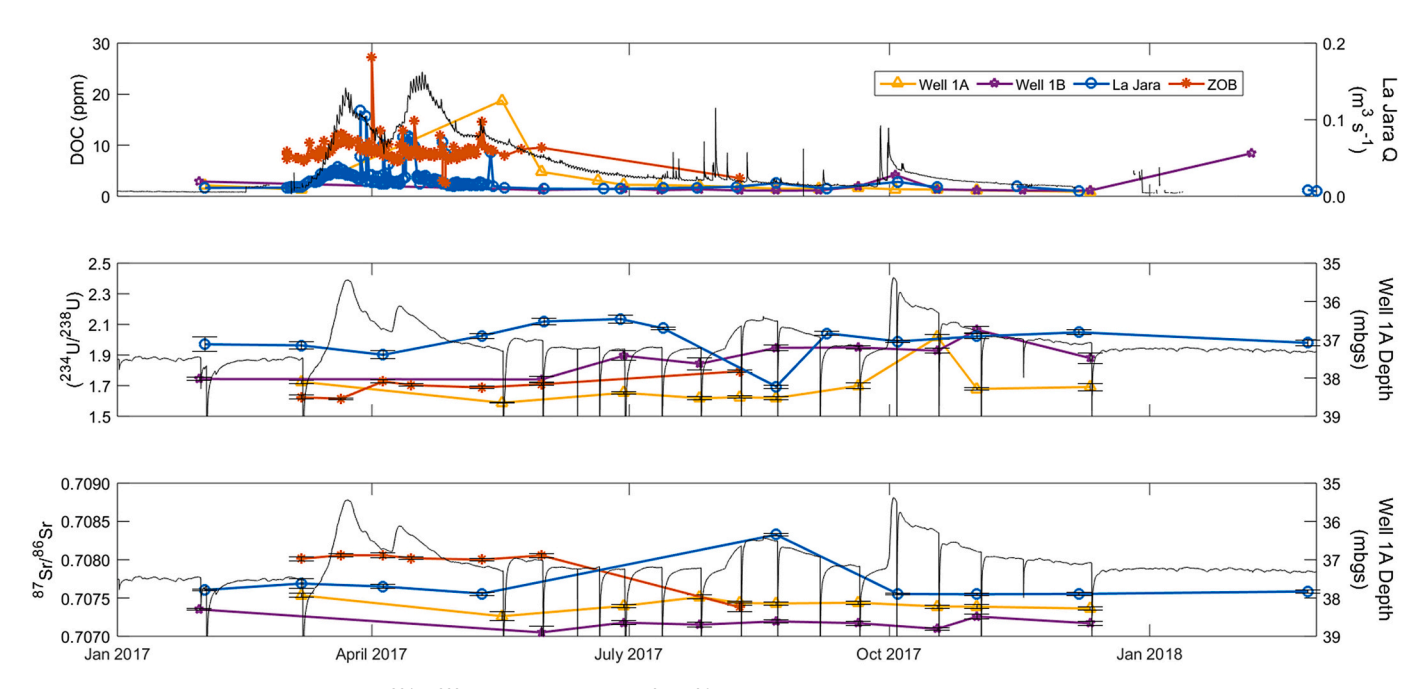


Fig. 8. Time series of DOC concentration, $(^{234}\text{U}/^{238}\text{U})$ activity ratios, and $^{87}\text{Sr}/^{86}\text{Sr}$ values of groundwater from Site 1 wells, La Jara surface water, and ZOB surface water. Geochemical analyses are shown over La Jara streamflow (top) and well 1A water table depth bgs (middle and bottom) for reference. Error bars for isotope values show internal precision (2 σ) of single measurements. Vertical lines in groundwater depth are the result of groundwater sampling.

variability of (²³⁴U/²³⁸U) and (²³⁰Th/²³⁸U) activity ratios observed in Site 1 core samples (Fig. 2A and B). We hypothesize that U-series weathering at Site 1 is less intense than that seen at Site 2 (Table 1) because of the homogenous nature of Site 1 lithology relative to that of Site 2, the absence of shallow groundwater at Site 1, and the flashy response of deep groundwater in the fractured tuff aquifer at Site 1 (White et al., 2019). We assert that the subsurface properties associated with these different lithologies, like a minimum porosity of approximately 0.4 in the first two meters below ground surface dropping sharply down to about 0.1 beneath 7 mbgs at Site 2 (Moravec et al., 2020), led to the presence of a shallow aquifer in breccia over vesicular tuff and the subsequent redistribution of U and Th throughout the profile. This leads to an open actively weathering system at Site 2 compared

to a more closed system in the low storage (White et al., 2019) deep fractured tuff aquifer of Site 1.

Little variation in ⁸⁷Sr/⁸⁶Sr values and Sr concentration with depth in Site 1 and 2 core samples deeper than 20 mbgs suggests that the deep tuff at both sites is similar in elemental composition (Table 1 and Fig. 5). In contrast, there is considerable variability in ⁸⁷Sr/⁸⁶Sr values and Sr concentrations in the top 20 mbgs of each site, which correspond to lithologic breaks in cores in the active weathering zone (Fig. 4). Further, a slightly elevated ⁸⁷Sr/⁸⁶Sr signature at 16 mbgs in Site 2 core is coincident with nearly 25% mass fraction of zeolites within the ash layer (Moravec et al., 2020) and a nearly 23-fold increase in Sr concentration relative to the above core sample. The ⁸⁷Sr/⁸⁶Sr signature and Sr concentration of Site 1 core increases with depth from the surface to

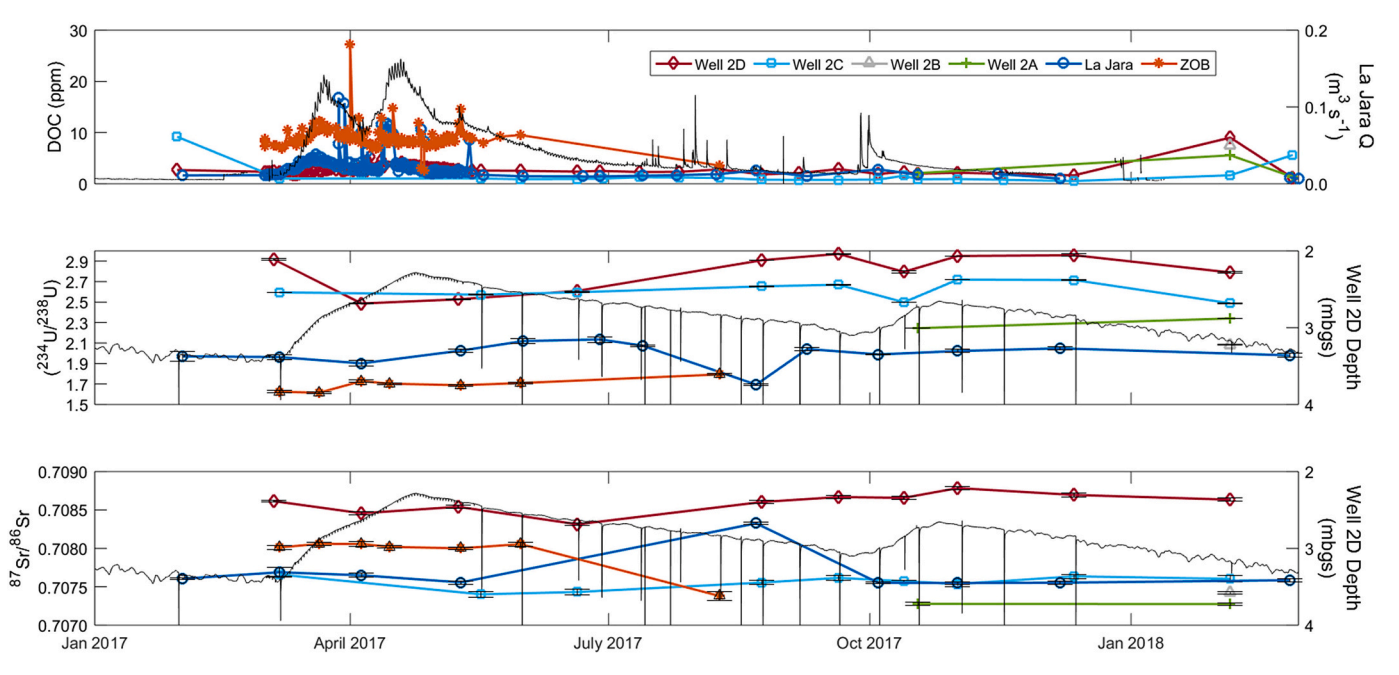


Fig. 9. Time series of DOC concentration, $(2^{34}\text{U}/2^{38}\text{U})$ activity ratios, and ${}^{87}\text{Sr}/{}^{86}\text{Sr}$ values of groundwater from Site 2 wells, La Jara surface water, and ZOB surface water. Geochemical analyses are shown over La Jara streamflow (top) and well 2D water table depth bgs (middle and bottom) for reference. Error bars for isotope values show internal precision (2σ) of single measurements. Vertical lines in groundwater depth are the result of groundwater sampling.

approximately 4 mbgs where both the Sr concentration and Sr isotope signature closely resemble that seen at 16 mbgs in Site 2 core, suggesting that Sr accumulates in zeolites at both sites; however, no trends in Ca/Sr versus ⁸⁷Sr/⁸⁶Sr values are evident (Supplemental Fig. 5), as would be expected with Ca-rich zeolites. Furthermore, the radiogenic Sr isotope signature of deep core from both sites closely resemble one another nearing ⁸⁷Sr/⁸⁶Sr values previously measured in Bandelier Tuff (0.7110) (Vuataz et al., 1988; Goff and Gardner, 1994).

4.2. Distinct U-series and Sr isotope signatures of groundwater stores

4.2.1. Evolution of U-series and Sr isotope signatures via water-rock interaction

 $(^{234}\mathrm{U}/^{238}\mathrm{U})$ activity ratios of all groundwater in the ZOB are greater than secular equilibrium, which demonstrates preferential release to solution of $^{234}\mathrm{U}$ during water-rock interactions (Porcelli and Swarzenski, 2003). In fact, $(^{234}\mathrm{U}/^{238}\mathrm{U})$ activity ratios of shallow groundwater and collocated rock (2.6 and 3.5 mbgs) from the shallow aquifer at well 2D are the most enriched and most depleted, respectively, suggesting that $^{234}\mathrm{U}$ is significantly leached from weathered rock into solution in the shallow aquifer. In this near surface environment, frequent and more enhanced weathering within the depth range of the well 2D water table (approximately 2.3 to 3.5 mbgs) likely exposes fresh surfaces to the most aggressive young water, allowing shallow groundwater to acquire a substantial $^{234}\mathrm{U}$ excess relatively quickly. Indeed, White et al. (2019) found that groundwater from well 2D was a mix of modern tritiated water (4.1 \pm 0.17 TU) and older water with approximately 75% modern radiocarbon.

It may be possible that the greater (²³⁴U/²³⁸U) activity ratios in this shallow groundwater store are related to the groundwater saturation or oversaturation with respect to calcite (Fig. 7A), while more radiogenic ⁸⁷Sr/⁸⁶Sr signatures of shallow groundwater are likely the result of interaction with radiogenic breccia rather than calcite saturation (Fig. 4 and 7B). U has been shown to be incorporated into or adsorbed onto surfaces of calcite (Chabaux et al., 2008), but U precipitation does not alter (²³⁴U/²³⁸U) activity ratios because of the large mass of these isotopes (Maher et al., 2004; Paces and Wurster, 2014). Furthermore, it is unlikely that U has been extensively removed from solution long enough

to impact (234 U/ 238 U) activity ratios through increased alpha recoil (Porcelli, 2008), as shown by U concentration of core samples coincident with calcite and the shallow groundwater table consistent with those of the deepest Site 2 core (Fig. 3D). The uranyl cation (UO_2^{2+}) forms soluble complexes with carbonate (Chabaux et al., 2003; Stewart et al., 2010) in the pH range of natural water like that observed here (Table 2); however, the relationship between calcite saturation index and $(^{234}\text{U}/^{238}\text{U})$ activity ratios does not appear to be linked solely to the concentration of Ca and DIC in solution because $(^{234}\text{U}/^{238}\text{U})$ activity ratios of Site 2 groundwater are not correlated with Ca or DIC content and U/Ca ratios are not correlated to (234U/238U) activity ratios in waters or solids (Supplemental Figs. 6 and 7). Perhaps, instead, both secondary precipitation of calcite and increased (²³⁴U/²³⁸U) activity ratios are the results of increased weathering-induced release of Ca²⁺ ions and exposure of fresh surfaces and finer grain size, both of which are known to increase the effect of alpha recoil (Chabaux et al., 2003). This would agree with the hypothesis from Moravec et al. (2020) that weathering of glass or plagioclase is likely the source of near surface calcite at Site 2; however, further analysis is required to unambiguously identify the calcite source.

Despite elevated (234U/238U) activity ratios of aquifer materials above and below the depth of well 2C groundwater (~28 mbgs; Fig. 5), (234U/238U) activity ratios of groundwater at this depth still have a considerable ²³⁴U excess, indicative of alpha recoil and subsequent preferential release of ²³⁴U. We hypothesize that U is transported to depth and continually renewed leading to U accumulation and enriched $(^{234}\text{U}/^{238}\text{U})$ and $(^{230}\text{Th}/^{238}\text{U})$ activity ratios at this depth where zeolites, known to strongly sorb U and Th (Chabaux et al., 2003; Porcelli, 2008), are present in large amounts (Fig. 3). Finally, (234U/238U) activity ratios of Site 1 groundwater stores are likely the result of alpha recoil and preferential release of ²³⁴U from fracture surfaces with a lesser degree of water-rock interaction than at Site 2 as Paces et al. (2002) suggested that welded tuff dissolution is slow and addition of ²³⁴U from preferential release outweighs release of ²³⁸U from dissolution. We speculate that Site 1 groundwater (234 U/ 238 U) activity ratios are lower than those of Site 2 because of faster, more frequent groundwater movement indicated by the flashier response and hydraulic connection of the fractured tuff aquifer to streamflow (White et al., 2019). This would imply that ²³⁴U is removed faster than it forms from decay and the time of waterrock interaction is limited. Furthermore, Moravec et al. (2020) found that fracture surfaces in Site 1 cores were armored with Fe and Mn oxides, which should act as physical barriers to primary mineral weathering.

4.2.2. Combination of U-series and Sr isotopes identifies distinct groundwater stores

(234U/238U) activity ratios and Log[U] depict distinct U signatures of Site 2 groundwater stores and Site 1 groundwater stores (Fig. 6A), which is corroborated by a past U-series study of springs from La Jara catchment that suggested distinct groundwater components - shallow groundwater with higher (234 U/ 238 U) activity ratios and deep groundwater with lower (234 U/ 238 U) activity ratios (Huckle et al., 2016). Furthermore, we find that La Jara and ZOB surface water (234U/238U) activity ratios and Log[U] overlap with those of Site 1 groundwater stores, suggesting that water from the fractured aquifer (i.e., deep CZ) at Site 1 is more representative of water contributing to streamflow, in agreement with past analysis of major ion chemistry from groundwater and surface water (White et al., 2019). However, there is some scatter in U signatures of each groundwater store and Johnson et al. (2000), Roback et al. (2001), and Paces et al. (2002) indicate that (234 U/ 238 U) activity ratios track water-rock interaction and water evolution along flowpaths but may not be a conservative indicator of lithology. Therefore, analysis of ⁸⁷Sr/⁸⁶Sr values was added to bolster this hypothesis.

The combination of these two radiogenic isotope tracers very clearly defines distinct isotope signatures of each groundwater store that can be used to quantify groundwater contribution to streamflow (Fig. 10). While the (234 U/ 238 U) activity ratios of rocks and collocated groundwater from both sites and all depths varies markedly, variations in 87 Sr/ 86 Sr values of rock and associated groundwater are considerably smaller, especially in deeper groundwater as Sr isotopes are known to be a conservative tracer of chemical weathering and, thus, hold the

signature of the tuff seen at depth in both sites. Furthermore, the lack of trends between \$^8Sr/^{86}Sr values and $(^{234}U/^{238}U)$ activity ratios of each groundwater store (Fig. 10) demonstrate that the isotope systems are influenced by different controls. This comparison reveals that U-series disequilibrium, while used at large scale to show groundwater contribution to rivers and trace elemental fluxes carried to rivers from different lithologies (Riotte and Chabaux, 1999; Bagard et al., 2011), is more strongly controlled by differences in subsurface structural properties of those lithologies (e.g., fracture density, groundwater storage, rate of groundwater movement) and the subsequent differences in water-rock interaction rather than the chemical composition of the aquifer (Sarin et al., 1990) as Sr isotopes only display minor differences across rock type and groundwater stores, which highlights the utility of combining these two isotope tracers.

4.3. U-series and Sr isotope tracers show temporal variability in surface and groundwater

Previous concentration-discharge analysis of snowmelt during 2017 in the JRB-CZO indicated that Sr is not associated with colloids (Olshansky et al., 2018), and (234U/238U) activity ratios (Porcelli et al., 1997; Riotte et al., 2003) and 87Sr/86Sr values (Banner and Hanson, 1990) have been shown to be independent of filtration size during sample processing. These observations, combined with the large mass of these isotope systems, which prevents isotopic fractionation during transport, adsorption, and evaporative concentration (Paces et al., 2002), make both isotope systems appropriate hydrologic tracers. 87Sr/86Sr values of both Site 1 groundwater stores (wells 1A and 1B) change simultaneously and remain close to one another year-round (Fig. 8), as expected since both water stores reside in fractured tuff with very little variability in mineralogy or 87Sr/86Sr values of core samples deeper than 13 mbgs (Fig. 4). However, the 87Sr/86Sr signature

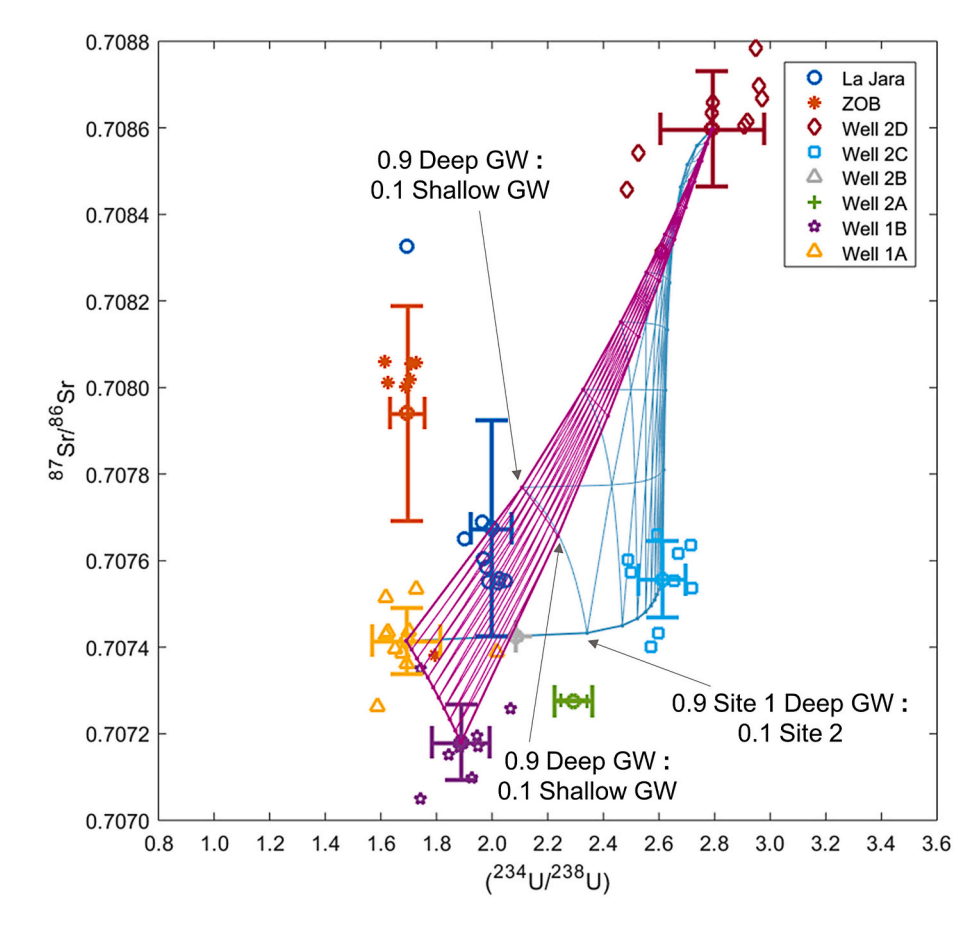


Fig. 10. 87 Sr/ 86 Sr values versus (234 U/ 238 U) activity ratios where mean concentrations for each water type are denoted as open circles between crosshairs showing one standard deviation for each isotope system. Two mixing spaces are shown with La Jara and ZOB surface waters bound by deep groundwater from wells 1A and 1B and shallow groundwater from well 2D (purple) and deep groundwater from well 1A, shallow groundwater from well 2D, and deeper groundwater from well 2C (blue). Thick lines represent mixing lines between two end members with dots marking fractions from 0.1 to 0.9. Thin lines are mixing lines between three end members spanning fractions of two end member lines. Average La Jara surface water is composed of greater than 90% deep groundwater from the fractured tuff aguifer at Site 1 and less than 10% groundwater from Site 2. Average ZOB surface water cannot be constrained with groundwater sources alone. (For interpretation of the references to colour in this figure legend, the reader is referred to the web version of this article.)

of Site 1 water (Table 2) is more radiogenic than the bulk Site 1 core in that depth range (Table 1) as is commonly seen in Sr isotope studies, possibly because of dissolution of more radiogenic minerals (Roback et al., 2001; Shand et al., 2009).

Furthermore, the drop in $(^{234}\text{U}/^{238}\text{U})$ activity ratios of Site 1 water following snowmelt is coincident with a DOC peak in Site 1 groundwater (Fig. 8), which likely indicates soil water input to the Site 1 fractured tuff aquifer system during snowmelt (Perdrial et al., 2014; Olshansky et al., 2018); however, without samples from that time period because of site inaccessibility this cannot be further investigated. We hypothesize that Site 1 $(^{234}\text{U}/^{238}\text{U})$ activity ratios are low, closer to the soil water $(^{234}\text{U}/^{238}\text{U})$ signature in the ZOB (average soil water $(^{234}\text{U}/^{238}\text{U})$ activity ratio of 1.368; Huckle et al., 2016) immediately following snowmelt while DOC concentrations are elevated, and activity ratios increase as DOC and associated soil water inputs cease. The subsequent rise in $(^{234}\text{U}/^{238}\text{U})$ signature of Site 1 water following snowmelt, particularly that from the shallow reservoir (well 1B), likely indicates increased weathering of fresh surfaces releasing excess ^{234}U to groundwater before $(^{234}\text{U}/^{238}\text{U})$ activity ratios return to baseflow values as the water table recedes.

Peaks of $(^{234}\text{U}/^{238}\text{U})$ activity ratios of groundwater from wells 2D and 2C are coincident with extremes in the well 2D water table depths where the lowest values were recorded from samples collected while the shallow groundwater table is rising (Fig. 9). In contrast to Site 1 wells, $(^{234}\text{U}/^{238}\text{U})$ activity ratios of Site 2 groundwater stores do not exceed baseflow values during peak flows and instead return to higher $(^{234}\text{U}/^{238}\text{U})$ activity ratios as the water table recedes to the depth coincident with the most depleted $(^{234}\text{U}/^{238}\text{U})$ activity ratio of core samples, suggesting that the $(^{234}\text{U}/^{238}\text{U})$ signature is lowered during recharge. The dip in well 2D groundwater $(^{234}\text{U}/^{238}\text{U})$ activity ratios during spring snowmelt and smaller dips during fall and winter are coincident with increases in DOC. This could indicate the impact of lower $(^{234}\text{U}/^{238}\text{U})$ activity ratios of actively recharging water since the $(^{234}\text{U}/^{238}\text{U})$ activity ratios of soil water in the ZOB range from 1.105 to 1.630 with an average soil water of 1.368 (Huckle et al., 2016).

Finally, surface water U-series and Sr isotope signatures of both La Jara and the ZOB are distinct from one another and vary over time (Figs. 8 and 9) due to seasonal differences in water routing. La Jara Useries and Sr isotope signatures are higher than those of deep groundwater from the fractured tuff aquifer at Site 1 during baseflow and spring snowmelt and always lower than those of shallow groundwater from Site 2, which suggests a mixture of groundwater stores from Sites 1 and 2 contribute to La Jara streamflow. For instance, shallow groundwater likely contributes most to streamflow during the period between spring snowmelt and the onset of summer monsoon rain when snowmelt infiltration induces shallow groundwater discharge to streamflow. During seasons of smaller shallow groundwater table response (summer and fall storms and winter baseflow; Fig. 9), shallow groundwater contribution to streamflow is suspected to decrease and the overwhelming majority of streamflow is hypothesized to come from deep groundwater from the fractured tuff aquifer with minimal contribution from shallow groundwater and a suspected soil water component. Furthermore, past U-series analysis found (234U/238U) activity ratios of La Jara springs (as proxies of groundwater) and surface water from a sampling event during spring snowmelt in May were 20% lower than those of a sampling event during November, which Huckle et al. (2016) suggested resulted from greater deep groundwater contribution to streamflow during snowmelt. However, with the addition of direct access to groundwater and longer, continuous time-series of U-series and Sr isotopes across seasons herein, we posit that the systematic difference in (234U/238U) activity ratios that Huckle et al. (2016) observed is instead due to greater soil water input associated with spring snowmelt. Our time-series of (234U/238U) activity ratios, 87Sr/86Sr, and DOC concentrations of groundwater and surface water (Figs. 8 and 9) indicate that deep groundwater sustains streamflow year-round. However, greater contributions of soil water and shallow groundwater (and

seasonally lower (234 U/ 238 U) activity ratios of shallow groundwater from soil water infiltration) to streamflow are observed during spring snowmelt and summer monsoons when soil moisture is greatest (White et al., 2019). Like La Jara streamflow, (234 U/ 238 U) activity ratios of ZOB streamflow are higher than those of deep groundwater from the fractured tuff aquifer at Site 1 and always lower than those of shallow groundwater from Site 2, again suggesting streamflow is a mixture of groundwater stores represented by Sites 1 and 2.

4.4. Quantifying groundwater contribution to streamflow using isotope mixing analysis

In order to quantify the relative contributions of groundwater stores from Sites 1 and 2 to streamflow, isotope mixing analysis was employed. Following the three component isotope mixing approach of Paces and Wurster (2014), streamflow sources were estimated from mixing analysis using mean values of ⁸⁷Sr/⁸⁶Sr, Sr concentration, (²³⁴U/²³⁸U) activity ratios, and U concentration of streamflow sources, or end members. For fractional mixing proportions of each end member ranging from 0 to 1 (0.1 fraction step shown in Fig. 10), the isotopic composition of the mixture is calculated for each isotope system. Mixing lines are hyperbolic rather than linear because the isotopic composition of the mixture is most strongly influenced by the end member with the highest elemental concentration (Faure, 1986); therefore, the degree of curvature of the hyperbolic mixing lines and the placement of fractional mixing proportions depends on the Sr and U concentrations of end members. As described by Paces and Wurster (2014), three end member mixing lines are produced as a series of separate two end member mixtures using classic two component mixing equations of Faure (1986) for fractional contributions of each member from 0 to 1 to create a mixing web (Fig. 10).

End members were identified by plotting triangular mixing spaces of three sources to bound surface water samples because, according to traditional mixing theory, if end members conservatively mix to produce the isotope signature of streamflow samples, then those samples will plot in the triangular space defined by its end members. However, if they plot outside of that space, an end member with a chemical signature closer to the unbound samples is missing (Christophersen et al., 1990; Hooper et al., 1990). Two mixing spaces (Fig. 10) capture the U-series and Sr isotope signatures of nearly all La Jara surface water samples. In both mixing spaces the average La Jara surface water falls on the mixing line between deep groundwater and shallow groundwater, indicating that deep groundwater from Site 1 contributes approximately 93% of La Jara streamflow and about 7% is contributed from Site 2 shallow groundwater. Furthermore, a range of greater than 90% to approximately 40% deep groundwater from well 1A and as much as 60% deep groundwater from well 1B are shown to contribute to La Jara streamflow (Fig. 10 in purple) while no more than 3% of groundwater from well 2C contributes to La Jara surface water (Fig. 10 in blue), suggesting that deep groundwater from both Site 1 fractured tuff wells and shallow groundwater are the most likely sources of the average La Jara streamflow (Fig. 10). Past studies using springs as proxies for groundwater, suggested that a combination of distinct shallow and deep groundwater contributes to La Jara stream (Huckle et al., 2016; McIntosh et al., 2017; Olshansky et al., 2018), which is consistent with our findings from U-Sr isotope mixing analysis. Furthermore, Huckle et al. (2016) showed that $(^{234}\mathrm{U}/^{238}\mathrm{U})$ activity ratios of longitudinal transects of La Jara stream water decrease with decreasing elevation across seasons suggesting that deep groundwater contribution to streamflow increases with decreasing elevation. Moreover, our isotope mixing analysis indicates that the vast majority of La Jara streamflow is sourced from groundwater in the deep CZ, which has been seen in other fractured tuff sites (Paces et al., 2002; Bushman et al., 2010), indicating that for deeply fractured bedrock systems, the deep CZ can dominate storage and flux of water resources in montane environments.

However, three streamflow samples – two from spring snowmelt (3/

7/2017 and 4/5/2017) and one from the summer monsoon season (8/ 22/17) plot outside of the groundwater only mixing space, suggesting that another source with a lower ($^{234}\text{U}/^{238}\text{U}$) activity ratio and a more radiogenic $^{87}\text{Sr}/^{86}\text{Sr}$ signature contributes to La Jara streamflow seasonally. We hypothesize that this additional source is soil water as Huckle et al. (2016) reported average soil water (234U/238U) activity ratios (1.368) lower than all components measured herein and Porter (2012) found radiogenic ⁸⁷Sr/⁸⁶Sr values of soils, similar to those of near surface core samples. Plus, previous analysis of volumetric water content in the ZOB during WY 2017 showed elevated soil moisture following the onset of spring snowmelt and late into the summer monsoon season (White et al., 2019), which is consistent with the timing of suspected soil water input to La Jara stream. ZOB streamflow samples are not captured in either mixing space, indicating that an end member with a higher ${}^{87}\text{Sr}/{}^{86}\text{Sr}$ and lower $({}^{234}\text{U}/{}^{238}\text{U})$ signature, similar to that expected of soil water likely contributes in greater quantities to ZOB streamflow compared to La Jara streamflow. This is consistent with a recent study of high frequency snowmelt 2017 surface, soil water, and groundwater samples that suggested that the carbon dynamics of ZOB surface water (pCO2, DIC, and DOC content) are influenced by those of soil water (Olshansky et al., 2018).

5. Conclusions

U-series activity ratios have emerged as a novel tracer of water-rock interaction and $^{87}{\rm Sr}/^{86}{\rm Sr}$ values are known to be a conservative tracer of chemical weathering. This study highlighted the utility of combining these two isotope systems for spatial analysis of solid and solution phase samples from collocated groundwater and cores collected from similar depths to indicate weathering processes in complex volcanic terrain. U-

series (²³⁸U–²³⁴U-²³⁰Th) and elemental ²³²Th isotopes pinpoint recent disturbances in U—Th equilibrium in Sites 1 and 2 while ⁸⁷Sr/⁸⁶Sr values show lithologic complexity in the near surface of both sites. However, weathering profiles of the fractured tuff core from Site 1 compared to the volcanic breccia overlying vesicular tuff core from Site 2 show more intense and complex weathering such as vertical transfer of U and Th down from the surface in Site 2 core samples likely influenced by the presence of shallow groundwater above deeper groundwater at Site 2 (Fig. 11). In addition, comparison of (²³⁴U/²³⁸U) activity ratios of groundwater stores and collocated core samples indicates that alpha recoil is the dominant process creating the ²³⁴U excess seen in all groundwater. Furthermore, this study shows that the combination of U-series and radiogenic Sr isotopes can trace groundwater contribution to streamflow because U-series and Sr isotope signatures identify distinct groundwater stores across sites and with depth.

Temporal analysis of U-series and Sr isotopes in surface water and groundwater inform water routing and U—Sr isotope mixing analysis estimates groundwater contribution to streamflow. Time series analysis of U-series and Sr isotope signatures and DOC content of groundwater and surface water indicate that the variability of isotope signatures of groundwater is thought to result from exposure of fresh surfaces and fracture coatings as the water table changes and from soil water infiltration to groundwater. While contribution from the Site 1 fractured aquifer system is expected to dominate La Jara streamflow year-round, shifts in the U-series and Sr isotope signature of surface water are hypothesized to indicate small seasonal changes in groundwater contribution with increased contribution from shallow groundwater to La Jara stream immediately following spring snowmelt. Furthermore, isotope mixing analysis estimates that groundwater from the fractured tuff aquifer system contributes approximately 93% to surface flows in the La

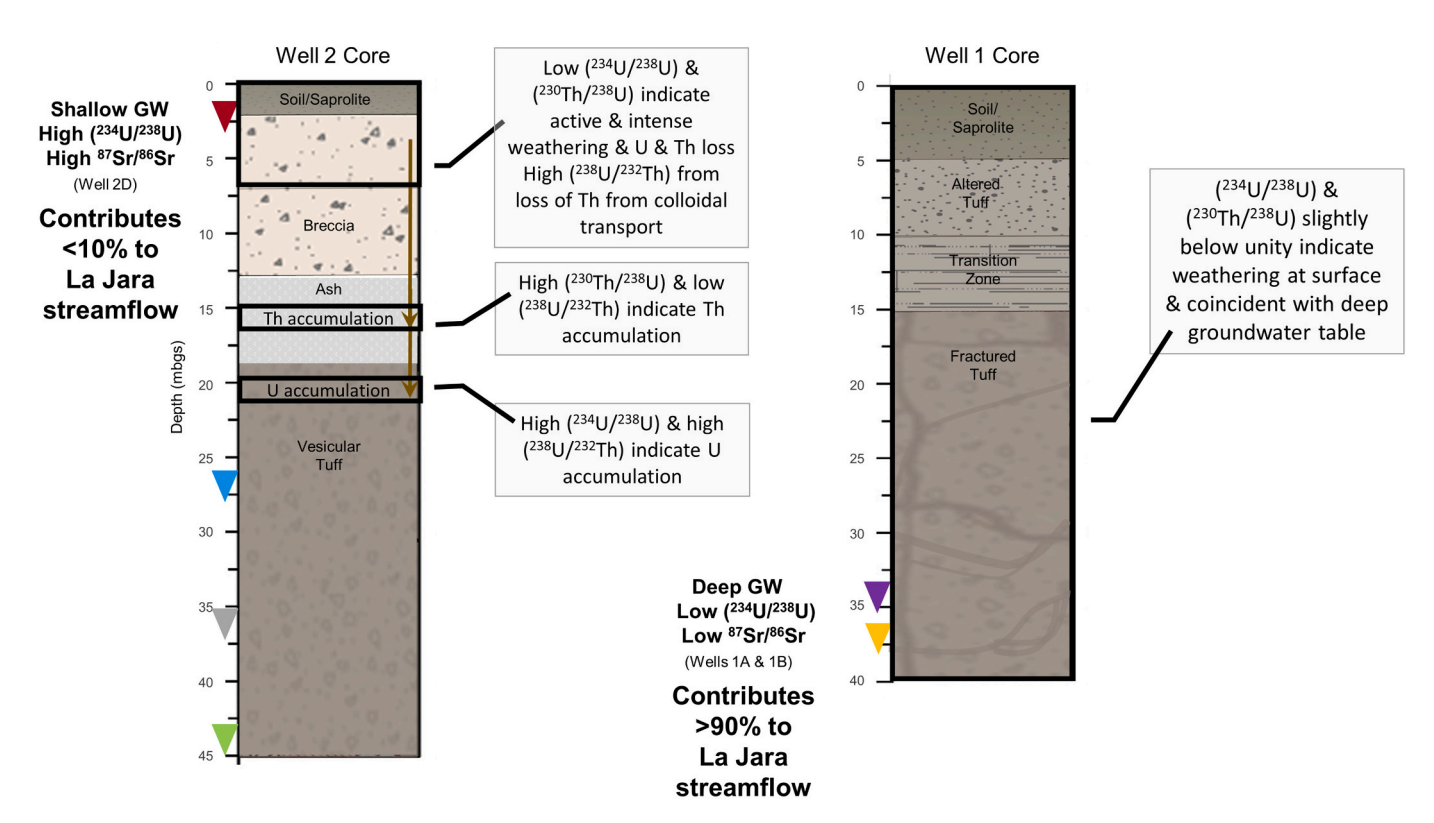


Fig. 11. Conceptual model detailing recent weathering in cores from U-series activity ratios and groundwater contribution to La Jara streamflow from U—Sr isotope mixing analysis. Weathering at Site 1 is limited throughout with only slight weathering in the near surface and coincident with the deep groundwater table (shown by inverted triangles). In contrast, weathering at Site 2 is influenced by the presence of organic-rich shallow groundwater, at which depth, weathering is active and intense and U and Th are lost from the near surface. Th is transported with colloids from the surface to depth and deposited at approximately 16 mbgs where colloids breakdown and U is deposited at approximately 21 mbgs where a large percentage of zeolites are present. While important for driving weathering and U and Th redistribution, shallow groundwater is not a large contributor to streamflow as it only comprises approximately 7% of average La Jara streamflow based on U-series and Sr isotope mixing analysis. Instead, average La Jara streamflow consists of greater than 90% groundwater from the deep fractured CZ seen at Site 1.

A. White et al. Chemical Geology 570 (2021) 120156

Jara catchment (Fig. 11). Results from this study demonstrate the utility of combining isotope tracers for mixing analysis and highlights the importance of groundwater from the deep CZ in sustaining streamflow in high elevation volcanic settings, such as those that provide water to large population centers downgradient in semi-arid environments like the American Southwest.

Supplementary data to this article can be found online at https://doi.org/10.1016/j.chemgeo.2021.120156.

Declaration of Competing Interest

None.

Acknowledgements

This work was supported by the National Science Foundation Division of Earth Sciences Jemez River Basin Critical Zone Observatory project (grants EAR-0724958 and EAR-1331408). L. Ma acknowledges research supported by NSF grant EAR-1349091. We would like to thank Mary Kay Amistadi, Danielle Barrientes, Tim Corley, and the filtering crew for their help processing samples in the University of Arizona labs, Matej Durcik for remote sensing analysis, and Mark Losleben and Adam Killebrew for their help with fieldwork.

References

- Andersson, P.S., Wasserburg, G.J., Chen, J.H., Papanastassiou, D.A., Ingri, J., 1995. 238U234U and232Th230Th in the Baltic Sea and in river water. Earth Planet. Sci. Lett. 130 (1–4), 217–234.
- Andersson, P.S., Porcelli, D., Wasserburg, G.J., Ingri, J., 1998. Particle transport of 234U-238U in the Kalix River and in the Baltic Sea. Geochim. Cosmochim. Acta 62 (3), 395-302
- Appelo, C.A.J., Postma, D., 2005. Geochemistry, Groundwater and Pollution, 2nd ed. CRC press, New York.
- Bagard, M.L., Chabaux, F., Pokrovsky, O.S., Viers, J., Prokushkin, A.S., Stille, P., Rihs, S., Schmitt, A., Dupré, B., 2011. Seasonal variability of element fluxes in two Central Siberian rivers draining high latitude permafrost dominated areas. Geochim. Cosmochim. Acta 75 (12), 3335–3357.
- Banner, J.L., Hanson, G.N., 1990. Calculation of simultaneous isotopic and trace element variations during water-rock interaction with applications to carbonate diagenesis. Geochim. Cosmochim. Acta 54 (11), 3123–3137.
- Barnett, T.P., Adam, J.C., Lettenmaier, D.P., 2005. Potential impacts of a warming climate on water availability in snow-dominated regions. Nature 438 (7066), 303.
- Beisner, K.R., Solder, J.E., Tillman, F.D., Anderson, J.R., Antweiler, R.C., 2020. Geochemical characterization of groundwater evolution south of Grand Canyon, Arizona (USA). Hydrogeol. J. 28 (5), 1615–1633.
- Brantley, S.L., Lebedeva, M.I., Balashov, V.N., Singha, K., Sullivan, P.L., Stinchcomb, G., 2017. Toward a conceptual model relating chemical reaction fronts to water flow paths in hills. Geomorphology 277, 100–117.
- Bushman, M., Nelson, S.T., Tingey, D., Eggett, D., 2010. Regional groundwater flow in structurally-complex extended terranes: an evaluation of the sources of discharge at Ash Meadows, Nevada. J. Hydrol. 386 (1–4), 118–129.
- Chabaux, F., Riotte, J., Dequincey, O., 2003. U-Th-Ra fractionation during weathering and river transport. Rev. Mineral. Geochem. 52 (1), 533–576.
- Chabaux, F., Bourdon, B., Riotte, J., 2008. U-series geochemistry in weathering profiles, river waters and lakes. Radioact. Environ. 13, 49–104.
- Chorover, J., Derry, L.A., McDowell, W.H., 2017. Concentration-Discharge Relations in the critical Zone: Implications for Resolving Critical Zone Structure, Function, and Evolution. Water Resour. Res. 53 (11), 8654–8659.
- Christophersen, N., Neal, C., Hooper, R.P., Vogt, R.D., Andersen, S., 1990. Modeling streamwater chemistry as a mixture of soilwater end-maembers - A step towards second-generation acidification models. J. Hydrol. 116, 307–320.
- Dequincey, O., Chabaux, F., Clauer, N., Sigmarsson, O., Liewig, N., Leprun, J.C., 2002. Chemical mobilizations in laterites: evidence from trace elements and 238U-234U-230Th disequilibria. Geochim. Cosmochim. Acta 66 (7), 1197–1210.
- Dralle, D.N., Hahm, W.J., Rempe, D.M., Karst, N.J., Thompson, S.E., Dietrich, W.E., 2018. Quantification of the seasonal hillslope water storage that does not drive streamflow. Hydrol. Process. 32 (13), 1978–1992.
- Dupré, B., Viers, J., Dandurand, J.L., Polve, M., Bénézeth, P., Vervier, P., Braun, J.J., 1999. Major and trace elements associated with colloids in organic-rich river waters: ultrafiltration of natural and spiked solutions. Chem. Geol. 160 (1–2), 63–80.
- Faure, G., 1986. Principles of Isotope Geology, 2nd ed. Wiley, New York.
- Flinchum, B.A., Steven Holbrook, W., Rempe, D., Moon, S., Riebe, C.S., Carr, B.J., Peters, M.P., 2018. Critical zone structure under a granite ridge inferred from drilling and three-dimensional seismic refraction data. J. Geophys. Res. Earth Surf. 123 (6), 1317–1343.
- Frisbee, M.D., Tolley, D.G., Wilson, J.L., 2017. Field estimates of groundwater circulation depths in two mountainous watersheds in the western US and the effect of deep

- circulation on solute concentrations in streamflow. Water Resour. Res. 53 (4), 2693–2715.
- Garcia, S., Louvat, P., Gaillardet, J., Nyachoti, S., Ma, L., 2020. Combining uranium, boron, and strontium isotope ratios (234U/238U, 11B, 87Sr/86Sr) to trace and quantify salinity contributions to Rio Grande river in Southwestern United States. Front. Water 2, 82.
- Gardiner, J.B., Capo, R.C., Newell, D.L., Stewart, B.W., Phan, T.T., Keating, E.H., Hakala, J.A., 2020. Tracking natural CO2 migration through a sandstone aquifer using Sr, U and C isotopes: Chimayó, New Mexico, USA. Int. J. Greenh. Gas Control 104. 103209.
- Goff, F., Gardner, J.N., 1994. Evolution of a mineralized geothermal system, Valles Caldera, New Mexico. Econ. Geol. 89 (8), 1803–1832.
- Goff, F., Gardner, J.N., Reneau, S.L., Kelley, S.A., Kempter, K.A., Lawrence, J.R., 2011.
 Geologic map of the Valles caldera, Jemez Mountains, New Mexico. New Mexico Bur
 Geol Min Res Geol Map 79.
- Granet, M., Chabaux, F., Stille, P., France-Lanord, C., Pelt, E., 2007. Time-scales of sedimentary transfer and weathering processes from U-series nuclides: clues from the Himalayan rivers. Earth Planet. Sci. Lett. 261 (3–4), 389–406.
- Grant, G.E., Dietrich, W.E., 2017. The frontier beneath our feet. Water Resour. Res. 53 (4), 2605–2609.
- Gustafson, J.R., Brooks, P.D., Molotc, N.P., Veatc, W.C., 2010. Estimating snow sublimation using natural chemical and isotopic tracers across a gradient of solar radiation. Water Resour. Res. 46 (12).
- Harmon, R.S., Rosholt, J.N., 1982. Igneous rocks. In: Uranium Series Disequilibrium: Applications to Environmental Problems.
- Hooper, R.P, Christophersen, N., Peters, N.E., 1990. Modeling streamwater chemistrAy as a mixture of soilwater end-membets An application to the Panola Mountain catchment, Georgia, USA. J. Hydrol. 116, 321–343.
- Huckle, D., Ma, L., McIntosh, J., Vázquez-Ortega, A., Rasmussen, C., Chorover, J., 2016. U-series isotopic signatures of soils and headwater streams in a semi-arid complex volcanic terrain. Chem. Geol. 445, 68–83.
- Johnson, T.M., Roback, R.C., McLing, T.L., Bullen, T.D., DePaolo, D.J., Doughty, C., Hunt, R.J., Smith, R.W., Cecil, L.D., Murrell, M.T., 2000. Groundwater "fast paths" in the Snake River Plain aquifer: radiogenic isotope ratios as natural groundwater tracers. Geology 28, 871–874.
- Kim, H., Dietrich, W.E., Thurnhoffer, B.M., Bishop, J.K., Fung, I.Y., 2017. Controls on solute concentration-discharge relationships revealed by simultaneous hydrochemistry observations of hillslope runoff and stream flow: the importance of critical zone structure. Water Resour. Res. 53 (2), 1424–1443.
- Klos, P.Z., Goulden, M.L., Riebe, C.S., Tague, C.L., O'Geen, A.T., Flinchum, B.A., Hartsough, P.C., 2018. Subsurface plant-accessible water in mountain ecosystems with a Mediterranean climate. Wiley Interdiscip. Rev. Water 5 (3), e1277.
- Konter, J.G., Storm, L.P., 2014. High precision 87Sr/86Sr measurements by MC-ICP-MS, simultaneously solving for Kr interferences and mass-based fractionation. Chem. Geol. 385, 26–34.
- Lebedeva, M.I., Brantley, S.L., 2013. Exploring geochemical controls on weathering and erosion of convex hillslopes: beyond the empirical regolith production function. Earth Surf. Process. Landf. 38 (15), 1793–1807.
- Liu, F., Parmenter, R., Brooks, P.D., Conklin, M.H., Bales, R.C., 2008. Seasonal and interannual variation of streamflow pathways and biogeochemical implications in semi-arid, forested catchments in Valles Caldera, New Mexico. Ecohydrol. Ecosyst. Land Water Process Interact. Ecohydrogeomorphol. 1 (3), 239–252.
- Ma, L., Chabaux, F., Pelt, E., Blaes, E., Jin, L., Brantley, S., 2010. Regolith production rates calculated with uranium-series isotopes at Susquehanna/Shale Hills Critical Zone Observatory. Earth Planet. Sci. Lett. 297 (1–2), 211–225.
- Maher, K., DePaolo, D.J., Lin, J.C.F., 2004. Rates of silicate dissolution in deep-sea sediment: in situ measurement using 234U/238U of pore fluids. Geochim. Cosmochim. Acta 68 (22), 4629–4648.
- Malov, A.I., 2018. Evolution of groundwater chemistry in coastal aquifers of the south-eastern White Sea area (NW Russia) using 14C and 234U-238U dating. Sci. Total Environ. 616, 1208–1223.
- McIntosh, R.P., Schaumberg, N., Perdrial, N.E., Harpold, N.E., Vázquez-Ortega, N.E., Rasmussen, N.E., Vinson, N.E., Zapata-Rios, N.E., Brooks, N.E., Meixner, N.E., Pelletier, N.E., Derry, N.E., Chorover, N.E., 2017. Geochemical evolution of the critical zone across variable time scales informs concentration-discharge relationships: Jemez river basin critical zone observatory. Water Resour. Res. 53, 4169–4196. https://doi.org/10.1002/2016WR019712.
- Moravec, B.G., White, A., Root, R., Sanchez, A., Paras, B., McGuffy, C., McIntosh, J., Pelletier, J., Carr, B., Holbrook, W.S., Chorover, J., 2020. Resolving deep critical zone architecture in complex volcanic terrain. J. Geophys. Res. Earth Surf. 125 (1) https://doi.org/10.1029/2019JF005189.
- Muldavin, E., Tonne, P., 2003a. A Vegetation Survey and Preliminary Ecological
 Assessment of Valles Caldera National Preserve, New Mexico: Report for Cooperative
 Agreement No. 01CRAG0014. University of New Mexico, Albuquerque.
- Muldavin, E., Tonne, P., 2003b. A Vegetation Survey and Preliminary Ecological Assessment of Valles Caldera National Preserve. Natural Heritage, New Mexico, Albuquerque.
- Navarro-Martinez, F., Garcia, A.S., Sánchez-Martos, F., Espasa, A.B., Sánchez, L.M., Perulero, A.R., 2017. Radionuclides as natural tracers of the interaction between groundwater and surface water in the River Andarax, Spain. J. Environ. Radioact. 180, 9–18.
- Neymark, L.A., Premo, W.R., Emsbo, P., 2018. Combined radiogenic (87Sr/86Sr, 234 U/238 U) and stable (δ88Sr) isotope systematics as tracers of anthropogenic groundwater contamination within the Williston BasinUSA. Appl. Geochem. 96, 11–23.

- Olshansky, Y., White, A., Moravec, B., McIntosh, J., Chorover, J., 2018. Subsurface pore water contributions to stream concentration-discharge relations across a snowmelt hydrograph. Front. Earth Sci. 6 (181) https://doi.org/10.3389/feart.2018.00181.
- Osmond, J.K., Cowart, J.B., 1976. The theory and uses of natural uranium isotopic variations in hydrology. Atomic Energy Rev. 14 (4), 621–679.
- Osmond, J.K., Ivanovich, M., 1992. Uranium-series mobilization and surface hydrology. In: Ivanovich, M., Harmon, R.S. (Eds.), Uranium Series Disequilibrium: Applications to Earth, Marine, and Environmental Sciences. Clarendon Press, Oxford, pp. 250-280
- Paces, J.B., Wurster, F.C., 2014. Natural uranium and strontium isotope tracers of water sources and surface water–groundwater interactions in arid wetlands–Pahranagat Valley, Nevada, USA. J. Hydrol. 517, 213–225.
- Paces, J.B., Ludwig, K.R., Peterman, Z.E., Neymark, L.A., 2002. 234 U/238 U evidence for local recharge and patterns of ground-water flow in the vicinity of Yucca Mountain, Nevada, USA. Appl. Geochem. 17 (6), 751–779.
- Pelt, E., Chabaux, F., Innocent, C., Navarre-Sitchler, A.K., Sak, P.B., Brantley, S.L., 2008. Uranium-thorium chronometry of weathering rinds: rock alteration rate and paleoisotopic record of weathering fluids. Earth Planet. Sci. Lett. 276 (1–2), 98–105.
- Perdrial, J.N., McIntosh, J., Harpold, A., Brooks, P.D., Zapata-Rios, X., Ray, J., Meixner, T., Kanduc, T., Litvak, M., Troch, P.A., Chorover, J., 2014. Stream water carbon controls in seasonally snow-covered mountain catchments: impact of interannual variability of water fluxes, catchment aspect and seasonal processes. Biogeochemistry 118 (1–3), 273–290.
- Porcelli, D., 2008. Investigating groundwater processes using U-and Th-series nuclides. Radioact. Environ. 13, 105–153.
- Porcelli, D., Swarzenski, P.W., 2003. The behavior of U-and Th-series nuclides in groundwater. Rev. Mineral. Geochem. 52 (1), 317–361.
- Porcelli, D., Andersson, P.S., Wasserburg, G.J., Ingri, J., Baskaran, M., 1997. The importance of colloids and mires for the transport of uranium isotopes through the Kalix River watershed and Baltic Sea. Geochim. Cosmochim. Acta 61 (19), 4095–4113
- Porcelli, D., Andersson, P.S., Baskaran, M., Wasserburg, G.J., 2001. Transport of U-and Th-series nuclides in a Baltic Shield watershed and the Baltic Sea. Geochim. Cosmochim. Acta 65 (15), 2439–2459.
- Porter, C., 2012. Solute Inputs to Soil and Stream Waters in a Seasonally Snow-Covered Mountain Catchment Determined Using Ge/Si, ⁸⁷Sr/⁸⁶Sr and Major Ion Chemistry: Valles Caldera. The University of Arizona, New Mexico.
- Rempe, D.M., Dietrich, W.E., 2014. A bottom-up control on fresh-bedrock topography under landscapes. Proc. Natl. Acad. Sci. 111 (18), 6576–6581.
- Rempe, D.M., Dietrich, W.E., 2018. Direct observations of rock moisture, a hidden component of the hydrologic cycle. Proc. Natl. Acad. Sci. 115 (11), 2664–2669.
- Riebe, C.S., Hahm, W.J., Brantley, S.L., 2017. Controls on deep critical zone architecture: a historical review and four testable hypotheses. Earth Surf. Process. Landf. 42 (1), 128–156.
- Riotte, J., Chabaux, F., 1999. (234 U/238 U) activity ratios in freshwaters as tracers of hydrological processes: the Strengbach watershed (Vosges, France). Geochim. Cosmochim. Acta 63 (9), 1263–1275.
- Riotte, J., Chabaux, F., Benedetti, M., Dia, A., Gérard, M., Boulègue, J., Etamé, J., 2003. Uranium colloidal transport and origin of the 234 U-238 U fractionation in surface waters: new insights from Mount Cameroon. Chem. Geol. 202 (3-4), 365-381.

- Roback, R.C., Johnson, T.M., McLing, T.L., Murrell, M.T., Luo, S., Ku, T.L., 2001. Uranium isotopic evidence for groundwater chemical evolution and flow patterns in the eastern Snake River Plain aquifer, Idaho. Geol. Soc. Am. Bull. 113 (9), 1133–1141
- Rovan, L., Lojen, S., Zuliani, T., Kanduč, T., Petrič, M., Horvat, B., Štrok, M., 2020. Comparison of uranium isotopes and classical geochemical tracers in Karst Aquifer of Ljubljanica River catchment (Slovenia). Water 12 (7), 2064.
- Sarin, M.M., Krishnaswami, S., Moore, W.S., 1990. Chemistry of uranium, thorium, and radium isotopes in the Ganga-Brahmaputra river system: Weathering processes and fluxes to the Bay of Bengal. Geochim. Cosmochim. Acta 54 (5), 1387–1396.
- Shand, P., Darbyshire, D.P.F., Love, A.J., Edmunds, W.M., 2009. Sr isotopes in natural waters: Applications to source characterization and water–rock interaction in contrasting landscapes. Applied Geochemistry 24 (4), 574–586.
- St. Clair, J., Moon, S., Holbrook, W.S., Perron, J.T., Riebe, C.S., Martel, S.J., Richter, D. D., 2015. Geophysical imaging reveals topographic stress control of bedrock weathering. Science 350 (6260), 534–538.
- Stewart, B.D., Mayes, M.A., Fendorf, S., 2010. Impact of uranyl—calcium—carbonato complexes on uranium (VI) adsorption to synthetic and natural sediments. Environ. Sci. Technol. 44 (3), 928–934.
- Szramek, K., McIntosh, J.C., Williams, E.L., Kanduc, T., Ogrinc, N., Walter, L.M., 2007. Relative weathering intensity of calcite versus dolomite in carbonate-bearing temperate zone watersheds: Carbonate geochemistry and fluxes from catchments within the St. Lawrence and Danube river basins. Geochem. Geophys. Geosyst. 8 (4).
- Thiel, K., Vorwerk, R., Saager, R., Stupp, H.D., 1983. 235 U fission tracks and 238U-series disequilibria as a means to study recent mobilization of uranium in Archaean pyritic conglomerates. Earth Planet. Sci. Lett. 65 (2), 249–262.
- Viers, J., Dupré, B., Polvé, M., Schott, J., Dandurand, J.L., Braun, J.J., 1997. Chemical weathering in the drainage basin of a tropical watershed (Nsimi-Zoetele site, Cameroon): comparison between organic-poor and organic-rich waters. Chem. Geol. 140 (3–4), 181–206.
- Vuataz, F.D., Goff, F., Fouillac, C., Calvez, J.Y., 1988. A strontium isotope study of the VC-1 core hole and associated hydrothermal fluids and rocks from Valles Caldera, Jemez Mountains, New Mexico. J. Geophys. Res. Solid Earth 93 (B6), 6059–6067.
- Welch, L.A., Allen, D.M., 2014. Hydraulic conductivity characteristics in mountains and implications for conceptualizing bedrock groundwater flow. Hydrogeol. J. 22 (5), 1003–1026.
- White, A., Moravec, B., McIntosh, J., Olshansky, Y., Paras, B., Sanchez, R.A., Ferre, T.P. A., Meixner, T., Chorover, J., 2019. Distinct stores and routing of water in the deep critical zone of a snow dominated volcanic catchment. Hydrol. Earth Syst. Sci. https://doi.org/10.5194/hess-2019-140.
- Wolff, J.A., Brunstad, K.A., Gardner, J.N., 2011. Reconstruction of the most recent volcanic eruptions from the Valles caldera, New Mexico. J. Volcanol. Geotherm. Res. 199 (1–2), 53–68.
- Zapata-Rios, X., McIntosh, J., Rademacher, L., Troch, P.A., Brooks, P.D., Rasmussen, C., Chorover, J., 2015. Climatic and landscape controls on water transit times and silicate mineral weathering in the critical zone. Water Resour. Res. 51, 6036–6051. https://doi.org/10.1002/2015WR017018.